Thesis

Role of NAD+ levels in Western Diet-induced atherosclerosis

submitted by

Thomas Rathner

In partial fulfillment of the requirements for the degree of

Doktor(in) der gesamten Heilkunde

(Dr. med. univ.)

at the

Medical University of Graz

executed at the

University Department of Internal Medicine

Division of Cardiology, University Heart Center Graz

under supervision of

Assoz. Prof. Priv.-Doz. Dr. med. Bugger, Heiko

Byrne, Nikole, PhD

Graz, 24.05.24

Declaration of Academic Integrity

I hereby confirm that the present diploma thesis is the result of my own independent scholarly work. I also confirm that in all cases, where material from the work of others (in books, articles, essays, dissertations, and on the internet) is acknowledged, quotations and paraphrases are clearly indicated. No material other than that cited in the reference list has been used. I have read and understood the Medical University's regulations and procedures concerning plagiarism.

Graz, 24.05.2024 *Thomas Rathner m.p.*

Acknowledgements

First, I would like to thank Assoz. Prof. Priv.-Doz. Dr. med. Heiko Bugger for the opportunity to join the Cardiac Energetics Laboratory, conduct research for my diploma thesis and for providing excellent mentoring. He always gave expert guidance and provided insights into up-to-date research topics. The regular discussion of research progress and challenges allowed me to solve problems and gave me an understanding how basic research works. Nikole Byrne, PhD not only taught me laboratory and research techniques but patiently discussed all questions I had. Her enthusiasm, knowledge and outstanding support enabled me to overcome challenges and made my work for the diploma thesis instructive and exciting.

I would like to extend gratitude to Dipl.-Biol. Katharina Pfeil for help, patience, and advice from experiment planning, learning lab techniques, optimization of protocols to analysis of the results. I have learned a lot from her outstanding experience and precision. I would also like to thank Nathaly Anto, PhD for advice regarding experiment planning, training for dissections and histology. Franz Cichoki helped during dissection and histological cutting. Dr. med. univ. Ivan Vosko gave helpful advice. Viktoria Trummer-Herbst, MSc supported animal caretaking and lab work. Furthermore, I thank the whole cardiovascular research unit for the warm welcome, integration in the team, the great working atmosphere and support I have received.

I want to acknowledge that the following experiments were not conducted by myself: Feeding of the mice, measurement of physiological data, iGTT, processing of the blood, and leukocyte isolation were predominantly done by Katharina Pfeil and Nikole Byrne. The RNA extracted was performed by Katharina Pfeil. NAD+ measurement was performed by Nikole Byrne. The Jess Western Blot system optimization and run was performed by Nikole Byrne and Carolin Költgen.

I would like to thank Fürst Dietrichstein Foundation for generous support throughout my medical studies. Finally, I would like to thank my family for their ongoing support, otherwise it would not have been possible.

Zusammenfassung

Hintergrund: Atherosklerose ist eine inflammatorische Erkrankung und die Hauptursache kardiovaskulärer Erkrankungen. Das Koenzym NAD+ ist im Metabolismus von zentraler Bedeutung, da es Wasserstoffionen und Elektronen transportiert, sowie als Substrat für eine Vielzahl an Enzymen dient. Eine reduzierte NAD+-Konzentration kann pro-inflammatorische Reaktionen auslösen und ist mit dem Fortschreiten der Atherosklerose assoziiert. NAD+-Vorstufen, wie Nicotinamid Mononucleotid (NMN), können in diversen Geweben die NAD+-Konzentration wiederherstellen. Das Ziel dieser Studie war, den Effekt einer NMN-Behandlung auf die Entstehung der Atherosklerose zu zeigen.

Methoden: Männliche acht Wochen alte C57BL/6J Low Density Lipoprotein Rezeptor Knockout ($Ldlr^{-/-}$) Mäuse wurden entweder mit einer Standarddiät (n=12) oder einer WD mit 1.25 % Cholesterin (n=12) gefüttert. Nach acht Wochen Diät wurde jeweils die Hälfte der Gruppe mit NMN im Trinkwasser behandelt (500 mg/kg/Tag). Es wurden Glukose-Toleranz-Tests (GTT), Lipidmessungen, Leukozyten-Isolation aus Knochenmark und Milz, NAD+-Messungen, Western Blots, RT-qPCR und Histologie von Aortenwurzel und Aortenbogen durchgeführt.

Resultate: Die Oil red O Färbung zeigte ausgeprägte Atherosklerose in den WD gefütterten Gruppen. NMN-Behandlung reduzierte diese Atherosklerose in der Aortenwurzel. Im Milzleukozyten waren die NAD+-Spiegel reduziert und die Expression von NAD+-produzierenden (*Nampt, Nmnat1*) und NAD+-konsumierenden Enzymen (*Parp1, Cd38, Sirt3*) erhöht. NMN-Behandlung normalisierte NAD+-Spiegel und die Veränderungen der Genexpression. Die Menge an acetylierter Mangan Superoxid Dismutase (Ac-MnSOD), ein Zielprotein der NAD+-abhängigen Deacetylase SIRT3, war nach WD erhöht. Die Expression der SIRT3-regulierten Inflammasomkomponente NLRP3 war in WD-gefütterten Mäusen erhöht, was durch NMN-Behandlung abgeschwächt wurde.

Diskussion: NMN-Behandlung mindert die Entwicklung einer Atherosklerose, was auf den Beitrag einer NAD+-Depletion in der Pathogenese der Atherosklerose hinweist. Möglicherweise werden diese Effekte durch reduzierte SIRT3-Aktivität und erhöhte Inflammasomaktivierung in Leukozyten vermittelt. NAD+-Supplementierung könnte daher eine vielversprechende Therapieoption zur Abschwächung oder Prävention der Atherosklerose sein.

Abstract

Background: Atherosclerosis is an inflammatory disease and a main contributor to cardiovascular death. The coenzyme nicotinamide adenine dinucleotide (NAD+) is of central importance in metabolism, as it transports hydrogen and electrons to the electron transport chain and acts as a co-substrate for several metabolic enzymes. It has been shown that NAD+ depletion induces a pro-inflammatory response and is associated with the progression of atherosclerosis. NAD+ precursors, such as nicotinamide mononucleotide (NMN), have been shown to replenish NAD+ levels in several tissues. The aim of this study was to demonstrate the effect of NMN-treatment on the development of atherosclerosis.

Methods: 8-week-old C57BL/6J male low density lipoprotein receptor knockout ($Ldlr^{-/-}$) mice were fed a chow diet or a western diet (WD) containing 1.25 % cholesterol. After 8 weeks of diet, half the mice from each diet were supplemented with NMN in the drinking water (500 mg/kg/day) (n=6 per group). We performed glucose tolerance tests, plasma lipid measurements, leukocyte isolation from bone marrow and spleen, NAD+ quantification, automated western blotting, RT-qPCR and Oil Red O staining of the aortic root and arch.

Results: Oil red O staining showed distinct atherosclerotic lesions in the WD-fed group. NMN-treatment significantly reduced atherosclerosis of WD-fed mice. NAD+ levels were significantly decreased in spleen leukocytes of WD-fed mice, accompanied by increased expression of NAD+-producing (*Nampt, Nmnat1*) and NAD+-consuming (*Parp1, Cd38, Sirt3*) enzymes. NMN treatment restored NAD+ levels and blunted the alterations in gene expression. Acetylation of manganese superoxide dismutase (MnSOD), a target of the NAD+-dependent deacetylase SIRT3, was increased in WD-fed mice, indicating reduced SIRT3 activity following WD feeding. WD also increased leukocyte expression of the SIRT3-regulated inflammasome component, NLRP3, an effect that was blunted in response to NMN treatment.

Conclusion: NMN treatment attenuated the development of atherosclerosis, indicating that NAD+ depletion contributes to atherosclerosis pathogenesis, possibly by impairing SIRT3 activity and amplifying NLRP3 activity in leukocytes. Thus, NAD+ supplementation may be a promising strategy to attenuate or prevent development of atherosclerosis.

Publication

At the time of submission, this thesis had not been published.

Table of Contents

1 List of abbreviations

(Ac-)MnSOD	Acetylated manganese superoxide dismutase
ACTB	Beta-actin
AMPK	5‘adenosine monophosphate-activated protein kinase
ApoB100	Apolipoprotein B-100
$Apoe^{-/-}$	APOE knockout mouse
ATGL	Adipose triglyceride lipase
AUC	Area under the curve
BM	Bone marrow
CD3	Cluster of differentiation 3
CD4	Cluster of differentiation 4, T helper cell
CD8	Cluster of differentiation 8, T killer cell
CD36	Cluster of differentiation 36, fatty acid translocase
CD38	Cluster of differentiation 38, cyclic ADP ribose hydrolase
CD68	Cluster of differentiation 68
cDNA	Complementary deoxyribonucleic acid
Cq	Quantification cycle
CVD	Cardiovascular disease
DAMP	Damage-associated molecular pattern
DNA	deoxyribonucleic acid
EDTA	Ethylendiamintetraacetic acid
eNAMPT/iNAMPT	Extracellular/intracellular nicotinamide phosphoribosyl transferase
ETC	Electron transport chain
FAD/FADH2	Flavin adenine dinucleotide oxidized/reduced form
FFA	Free fatty acid
FOXO3a	Forkhead box O3a
FOXP3	Forkhead box P3
GLUT1	Glucose transporter 1
GM-CSF	Granulocyte-macrophage colony-stimulating factor
HDL	High-density lipoprotein
HFD	High-fat diet
HIF-1-α	Hypoxia-inducible factor 1-alpha

HMGCS2	3-hydroxymethylglutaryl-CoA synthase 2
HPRT	Hypoxanthine phosphoribosyltranferase 1
HRP	Horseradish peroxidase
IDH2	Isocitrate dehydrogenase 2
IDL	Intermediate-density lipoprotein
IDO1	Indoleamine 2,3-Dioxygenase 1
IFN-γ	Interferon gamma
IgG	Immunglobulin G
iGTT	Intraperitoneal glucose tolerance test
IL-1β, -3, -4, -6, -10, -13	Interleukin-1 beta, -3, -4, -6, -10, 13
LCAD	Long chain acyl-CoA dehydrogenase
LDL	Low-density lipoprotein
$Ldlr^{-/-}$	LDL receptor knockout mouse
LOX-1	Lectin-type oxidized low density lipoprotein receptor 1
LPS	Lipopolysaccharides
M1	Pro-inflammatory macrophage phenotype
M2	Anti-inflammatory macrophage phenotype
mRNA	Messenger ribonucleic acid
mTOR	Mammalian target of rapamycin
mTORC	Mammalian target of rapamycin complex 1
NA	Nicotinic acid
NAAD	Nicotinic acid adenine dinucleotide
NAD+/NADH	Nicotinamide adenine dinucleotide oxidized form/reduced form
NADP+/NADPH	Nicotinamide adenine dinucleotide phosphate oxidized/reduced form
NAM	Nicotinamide
NAMN	Nicotinate mononucleotide
NF-κB	Nuclear factor-kappa B
NIR	Near-infrared
NLRP3	NLR family pyrin domain containing 3
NMN	Nicotinamide mononucleotide

NMNAT1-3	Nicotinamide mononucleotide adenylyl transferase 1-3
NR	Nicotinamide riboside
Mac3	Macrophage differentiation antigen/CD107b/LAMP-2
OCT	Optimal cutting temperature compound
oxLDL	Oxidized low-density lipoprotein
oxPL	Oxidized phospholipids
PBMC	Peripheral blood mononuclear cells
PARP1	Poly ADP-ribose polymerase 1
PAMP	Pathogen-associated molecular pattern
PBS	Phosphate buffered saline
PCSK9	Proprotein convertase subtilisin/kexin type 9
PDHA1	pyruvate dehydrogenase E1 alpha
QA	Quinolinic acid
QPRT	Quinolinate phophoribosyl transferase
ROS	Reactive oxygen species
RPLP0	Ribosomal protein lateral stalk subunit P0
RT	Reverse transcriptase
RT-qPCR	Quantitative reverse transcription polymerase chain reaction
SDH	Succinate dehydrogenase
SEM	Standard error of the mean
SIRT1-7	Sirtuin 1-7
SR-AI/-AII	scavenger receptor class AI/AII
SR-BI	scavenger receptor class B member 1
TC	Total cholesterol
TCA	Tricarboxylic acid cycle
TG	Triglyceride
TGF-β	Transforming growth factor-beta
Th1	T helper cell subset 1
Th2	T helper cell subset 2
Th17	T helper cell subset 17
TLR	Toll-like receptor
TNF-α	Tumor necrosis factor alpha

Treg	T regulatory cell
UCP2	Uncoupling protein 2
Veh	Vehicle treatment
VLDL	Very low-density lipoprotein
WAT	White adipose tissue
WD	Western diet
18S	18s ribosomal ribonucleic acid

2 List of figures

3 List of tables

4 Introduction

4.1 Definition of atherosclerosis

Atherosclerosis is a chronic inflammatory process with deposition of fatty and/or fibrous material in the intima layer of arteries. It is the main cause of cardiovascular disease (CVD). Low-density-lipoprotein (LDL)-cholesterol plays a central role in the pathogenesis both in its native and oxidized form. LDL is deposited at areas with endothelial stress, accumulation of cholesterol occurs, and specific and unspecific immune reactions further drive the development of atherosclerosis (Libby, 2021).

4.2 Public health

CVDs, such as ischemic myocardial infarction and ischemic stroke, are globally a leading cause of mortality and morbidity. According to Eurostat, CVDs are by far the most common cause of death in the EU, accounting alone for 1/3 of all deaths in 2020 (Eurostat, 2023).

5 Background

5.1 Mouse models of atherosclerosis

During the last decades, mice were regularly used to study atherosclerosis. Unlike in humans, where diet contributes to the development of atherosclerosis, mice do not exhibit atherosclerotic plaques in response to high-fat or high-cholesterol feeding alone. Thus, it is important to note that mice do not develop atherosclerosis without genetic modifications, and often high-fat and/or high cholesterol western diet (WD) is additionally required. Moreover, mice do not exhibit intraplaque haemorrhage and do not normally develop late stages of atherosclerosis such as late fibroatheroma or fibrous calcified plaques, as occurs in humans (van Dijk et al., 2023).

Genetic knockout of apolipoprotein E ($Apoe^{-/-}$) or LDL receptor ($Ldlr^{-/-}$) are the most commonly used preclinical models for the study of atherosclerosis. For the following thesis, unless stated otherwise, knockout refers to a global inactivation of both alleles. The $Apoe^{-/-}$ model shows severe hypercholesterinemia and distinct atherosclerosis even on chow diet beyond the age of 16 weeks. $Apoe^{-/-}$ has especially increased very low-density lipoprotein-levels (VLDL), increased LDL, and

reduced high-density lipoprotein (HDL). In comparison, human dyslipidemia is typically characterized by increased LDL levels and reduced HDL levels, whereas only a small fraction of non-HDL cholesterol is VLDL (Plump et al., 1992). Loss of ApoE in mice has direct effects on inflammation, such as anti-inflammatory effect on lymphocytes and antigen presenting cells, and antioxidant activity against oxidized low-density lipoprotein (oxLDL) formation (Getz and Reardon, 2009).

Unlike Apoe$^{-/-}$ mice, Ldlr$^{-/-}$ mice exhibit only moderate hypercholesterinemia on chow diet and atherosclerosis is only observed with the addition of WD (Ishibashi et al., 1994a). WD aims to resemble the typical diet of industrialized countries, consisting of 0.15-1.25 % cholesterol and 15-20 % fat (Lichtman et al., 1999, Teupser et al., 2003). It is important to note that the cholesterol content of murine WD is extremely high compared to human diet. For example, even cholesterol rich human food contains below 0.4 % of cholesterol (Kuang et al., 2018). An average inhabitant of the western world consumes between 200-350 mg of cholesterol a day, which would be the equivalent of 16-28 g of WD containing 1.25 % cholesterol, (Carson et al., 2020), up to 10 times the food intake of mice in our study. It was shown that following WD, mice have increased levels of LDL, intermediate-density lipoprotein (IDL) and unchanged HDL (Ishibashi et al., 1994a). Crossing of Ldlr$^{-/-}$ mice with Apoe$^{-/-}$ mice yields a double knockout model exhibiting a severe phenotype even with chow diet, where both LDL and VLDL are dramatically increased and HDL is reduced (Ishibashi et al., 1994b).

Another, less common, pre-clinical model of atherosclerosis is the PCSK9 model, which used a single adenovirus infection to transfer the pro-atherogenic proprotein convertase subtilisin/kexin type 9 (Pcsk9) gene to the liver. These mice showed a phenotype comparable to Ldlr$^{-/-}$ mice (Roche-Molina et al., 2015). For the current study, we chose the Ldlr$^{-/-}$ model because WD-feeding most closely resembles diet-induced atherosclerosis in humans, as well as the observed elevated LDL-cholesterol and reduced HDL resembles the changes observed in humans.

5.2 Development of atherosclerosis

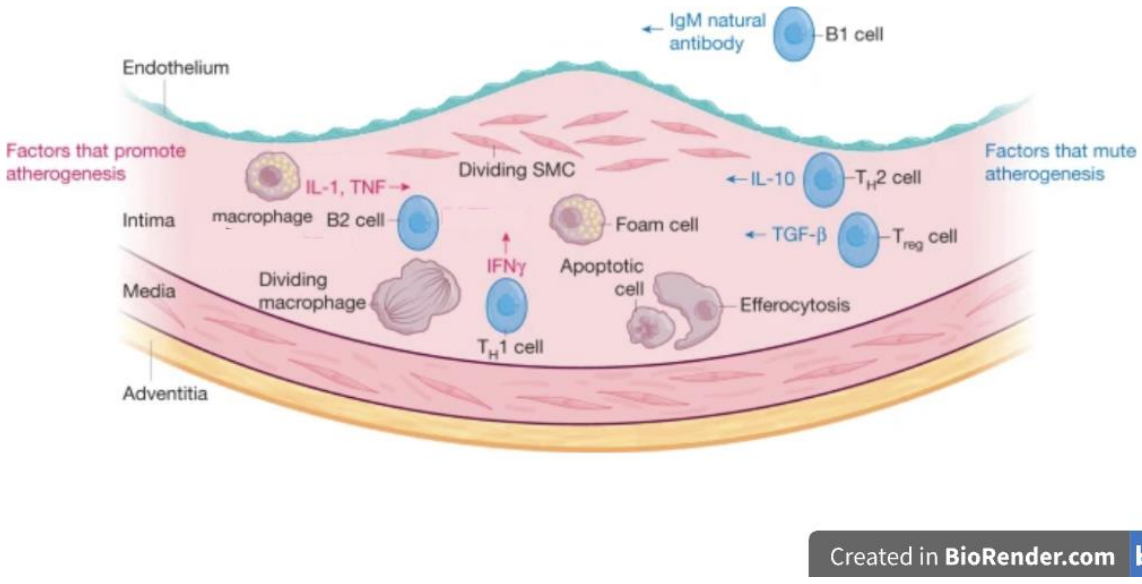

Figure 1: Overview of the development of atherosclerosis. Both innate and adaptive immune system are driving factors of the development of atherosclerosis. Adapted from Libby, 2021. Created with BioRender.com. IL-1, interleukin 1; TNF, tumor necrosis factor; IFN-γ, interferon gamma; IL-10, interleukin 10; TGF-β, transforming growth factor beta; Treg, T-regulatory cell.

The lining layer of endothelial cells of vessels ensure uncompromised blood flow. Risk factors such as hypertension, diabetes, smoking, inflammation, obesity can either affect vessels by mechanical stress or indirectly by mediating pro-inflammatory stimuli. Diabetes significantly increases the frequency and severity of the development of atherosclerosis, in part. mediated by the accumulation of glycosaminoglycans in the vessel walls (Renard et al., 2004). These effects lead to increased expression of molecules for leukocyte adhesion, resulting in a recruitment of immune cells to the subendothelial space (Franck et al., 2018).

Increased circulating LDL leads to the deposition of LDL particles in the intima. Transcytosis of LDL through the endothelium is a major component of lipid deposition (Zhang et al., 2018b). Sustained accumulation of LDL is a key factor for the development of atherosclerosis in both human and mice (Lewis et al., 2023, Tabas et al., 2007). Several reactive oxygen species (ROS) producing systems such as nicotinamide adenine dinucleotide phosphate (NADPH)-oxidase, xanthin oxidase, uncoupled nitric oxide synthase, and mitochondrial dysfunction contribute to the oxidation of LDL and phospholipids (Förstermann et al., 2017). The oxidation of LDL and phospholipids are pro-atherogenic (Que et al., 2018). The oxidized particles act as epitopes for damage-associated molecular patterns (DAMPs) (Miller et al., 2011). OxLDL and oxidized phospholipids (oxPL) are bound and internalized

by scavenger receptors on macrophages, such as fatty acid translocase (CD36), scavenger receptor class AI/AII (SR-AI, -AII), scavenger receptor class B member 1 (SR-BI) and lectin-type oxidized low density lipoprotein receptor 1 (LOX-1) (Moore and Freeman, 2006). OxLDL binding and uptake by CD36 activates a signal cascade leading to enhanced lipid uptake and foam cell formation (Rahaman et al., 2006). CD36 binding mediates a metabolic shift in macrophages from oxidative phosphorylation to ROS production which drives chronic inflammation (Chen et al., 2019). The uptake of oxLDL provokes formation of cholesterol crystals. These crystals drive NLR family pyrin domain containing 3 (NLRP3) inflammasome activation and pro-inflammatory IL-1β release (Sheedy et al., 2013, Duewell et al., 2010, Rajamäki et al., 2010). WD triggers innate immune reprogramming and facilitates chronic inflammation, mediated by NLRP3 (Christ et al., 2018). Exposure of endothelial cells to oxPL caused the release of chemoattractants. Among others, blood monocytes are recruited, which could intrude in the subintimal layers and differentiate to macrophages (Leitinger et al., 1999). Resident smooth muscle cells in the intima or smooth muscle cells from the media may undergo metaplasia and display a foam cell phenotype. Smooth muscle cells contribute to a deposition of extracellular matrix. In older atherosclerotic mice, the majority of foam cells are derived from smooth muscle cells and not from macrophages (Wang et al., 2019). Similarly, in humans it is shown that 40% of the coronary plaques' foam cells are of smooth muscle origin (Allahverdian et al., 2014).

Over time, the plaque accumulates more fibrous materials and calcification may occur. Newer studies in humans suggest that the progression is discontinuous and has an individual dynamic (Fracassi et al., 2019). The increase in plaque size may lead to vessel occlusion, especially if the surface of the plaque is unstable, plaque rupture may occur. A plaque rupture uncovers collagen on the surface and leads to activation of the blood clotting cascade and subsequent formation of thrombosis. Necrosis of foam cells and smooth muscle cells can trigger the formation of a necrotic core and increases plaque vulnerability (Clarke et al., 2006, Puylaert et al., 2022). It is important to note that a major difference between mice and human is that even atherosclerotic mice rarely suffer from plaque rupture and thrombotic complications (Hartwig et al., 2015). Plaque haemorrhage, often due to neoangiogenesis, starting from adventitial vasa vasorum in the plaque, is a major

cause of plaque vulnerability (Virmani et al., 2005). The affection of coronary arteries provokes cardiac ischemia and myocardial infarction. If a thrombus is carried away with the blood flow, arterial embolism may occur, often inducing stroke, other organ infarctions, and peripheral infarction, such as in the arteries of lower extremities (Rothwell et al., 2005, Herrington et al., 2016).

5.3 Clinical validation of the inflammation hypothesis

There have been several clinical studies proving the importance of inflammation in the development of atherosclerosis. In 2017, the large-scale multicentre randomized double-blinded placebo-controlled CANTOS trial was published (Ridker et al., 2017). In this trial the monoclonal antibody Canakinumab binding to IL-1β was administered after myocardial infarction and elevated inflammation marker C-reactive protein. The treatment significantly reduced cardiovascular complications during the study (Ridker et al., 2017). In 2013 and 2019, large scale multicentre randomized double-blinded placebo controlled LoDoCo and COLCOT trials were also published (Nidorf et al., 2013, Tardif et al., 2019). Here, the low dose treatment of the anti-inflammatory drug colchicine significantly reduced the incidence of cardiovascular complications in patients with stable coronary disease and after myocardial infarction (Nidorf et al., 2013, Tardif et al., 2019).

5.1 NAD+ metabolism

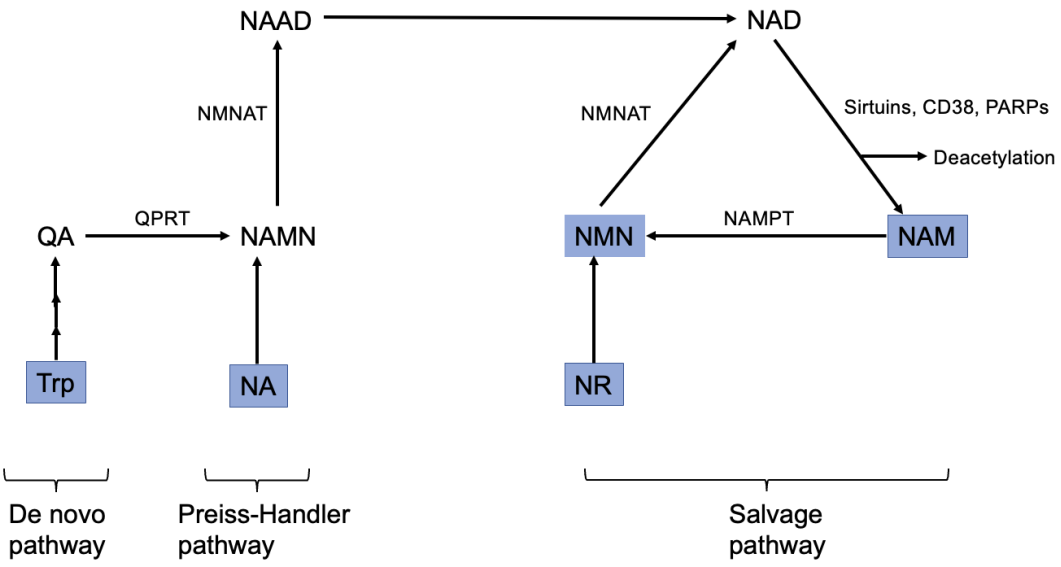

Figure 2: Overview of NAD+ metabolism. NAD+ can be either synthesised by the de novo pathway, Preiss-Handler pathway or reused by the salvage pathway. NAD+ is utilized by several enzymes such as sirtuins,

CD38, PARPs. Adapted from Srivastava, 2016. CD38, cluster of differentiation 38, cyclic ADP ribose hydrolase; NA, nicotinic acid; NAAD, nicotinic acid adenine dinucleotide; NAM nicotinamide; NAMN, nicotinate mononucleotide; NAMPT, nicotinamide phosphoribosyl transferase; NR, nicotinamide riboside; PARPs, poly ADP-ribose polymerase; QA, quinolinic acid; QPRT, quinolinate phophoribosyl transferase; Trp, tryptophan.

Nicotinamide adenine dinucleotide (NAD+/NADH) is of central importance for intracellular transport of electrons and protons. Additionally, it is a substrate for several important enzymes. NAD+ can be reduced to NADH by acceptation of 2 electrons and a proton. The ratio of NAD+/NADH and flavin adenine dinucleotide (FAD/FADH2) have a major influence on the redox state of cells. NAD+ is reduced during glycolysis and the tricarboxylic acid (TCA) cycle, then recovery by oxidation at the complex I of the mitochondrial electron transport (ETC) chain (Warburg and Christian, 1936, Amjad et al., 2021). There are three pathways for the synthesis of NAD+ (see overview in Fig. 2). The *de novo* synthesis starts from the amino acid tryptophan, encompasses the kynurenine pathway, intermediate quinolonic acid is converted by quinolinate phosphoribosyl transferase (QPRT) to nicotinate mononucleotide (NAMN) which is converted by nicotinamide mononucleotide adenylyl transferase 1-3 (NMNAT1-3) to NAD+ (Ijichi et al., 1966). In the Preiss-Handler pathway, nicotinic acid (NA), from food or produced by the microbiome, is converted to NAMN and then to NAD+ (Preiss and Handler, 1957). In the salvage pathway, NAD+ is utilized (e.g. by poly ADP-ribose polymerase (PARPs) or sirtuins), then is converted to nicotinamide (NAM). NAM is converted to nicotinamide mononucleotide (NMN) by NAMPT. NMNAT1-3 turns NMN into NAD+, thus the cycle is closed (Collins and Chaykin, 1972, Houtkooper et al., 2010). All enzymes involved in NAD+ synthesis are located in the cytosol. The only exception is NMNAT3 which is mitochondrial. However, a study in cultured human embryonic kidney cells questioned the expression of NMNAT3 in mitochondria and its role in maintenance of the mitochondrial NAD+ pool (Felici et al., 2013). NMN is a precursor of NAD+, which is rapidly taken up. The transport to the intracellular compartment can be either direct or by extracellular conversion to NR and intracellular reconversion to NMN. Intracellular NMNAT1-3 convert NMN to NAD+, thereby increasing the intracellular NAD+ level (Abdellatif et al., 2021, Yoshino et al., 2018, Nikiforov et al., 2011).

Extracellular NAMPT (eNAMPT) is secreted by a variety of cell types, for example by adipocytes. eNAMPT has pro-inflammatory functions and promotes macrophage

survival and skewing towards M1 phenotype (Li et al., 2008, Colombo et al., 2022). Intracellular NAMPT (iNAMPT) is important to maintain NAD+ levels and phagocytotic macrophage function (Venter et al., 2014). Global overexpression of iNAMPT reduced atherosclerosis in mice (Bermudez et al., 2017). It was shown that pharmacological NAMPT inhibition reduced NAD+ levels and inflammation, mediated by reduced activity of NAD+ dependent enzymes such as PARP1 in a murine model of liver ischemia-reperfusion (Lu et al., 2023). In macrophages stimulated with lipopolysaccharides, ROS led to deoxyribonucleic acid (DNA) damage, which increased PARP1 activity (Cameron et al., 2019). PARP1 depleted the NAD+ pool and NAMPT expression was increased in compensation (Cameron et al., 2019). It was shown that the NAD+ precursor, NAM, inhibited TNF-α synthesis in cultured murine macrophages (Van Gool et al., 2009). The treatment of heart failure patients with the NAD+ precursor nicotinamide riboside (NR) reversed the increased pro-inflammatory cytokine expression and impaired mitochondrial respiration in PBMC (Zhou et al., 2020).

Aging leads to a depletion of NAD+ through increased activity of PARP1 and other enzymes with NADase activity. These enzymes are closely related to inflammation, which is believed to be one factor of the frequent occurrence of inflammatory disease in the elderly (Massudi et al., 2012, McReynolds et al., 2020). One major contributor to the age dependent NAD+ decline was the increased activity of the NAD+ consuming enzyme, cyclic ADP ribose hydrolase (CD38), whereas other NAD+ consuming enzymes such as SIRT1 and PARP1 declined during aging (Camacho-Pereira et al., 2016). CD38 expression inversely regulated mitochondrial function (Camacho-Pereira et al., 2016). It was shown that CD38 inhibition increased NAD+ levels and ameliorated age-related metabolic dysfunction (Tarragó et al., 2018). CD38 was upregulated in endothelial cells as a response to pro-inflammatory IL-1β release (Qiu et al., 2023). This CD38 upregulation induced significant NAD+ depletion in both PBMC and aortic tissue during hypertension and vascular dysfunction in humans and mice (Qiu et al., 2023). Altogether, several studies have shown that NAD+ levels decline with aging, due to increased activity of NAD+ consuming enzymes.

5.1 Sirtuins

Sirtuins are NAD+ dependent deacetylases involved in the regulation of metabolism. There are Sirt1-7 with different functions. All sirtuins are homologues of the highly conserved Sir2 gene, first described in yeast (Imai et al., 2000). SIRT 3, 4, 5 are located in mitochondria, SIRT6 in nucleus, SIRT7 in nucleolus, and SIRT1 and 2 can shuttle between nucleus and cytosol (Grootaert and Bennett, 2022).

SIRT1: SIRT1 is involved in DNA repair, telomere maintenance and regulates transcription of manganese superoxide dismutase (MnSOD). SIRT1 inhibited pro-inflammatory Nuclear factor-kappa B (NF-κB) signalling. In humans it was shown that insulin resistance and subclinical atherosclerosis were associated with SIRT1 downregulation in monocytes (de Kreutzenberg et al., 2010). In human atherosclerotic plaques SIRT1 was downregulated (Gorenne et al., 2013). Overexpression of SIRT1 in endothelial cells reduced the development of atherosclerosis in mice (Zhang et al., 2008).

SIRT2: SIRT2 promoted MnSOD expression by deacetylation of the promoter forkhead box O3a (FOXO3a) and regulated DNA damage repair. (Zhang et al., 2016, Brunet et al., 2004). SIRT2 inhibited atherosclerotic plaque formation by inhibiting macrophage polarization towards M1 macrophages (Zhang et al., 2018a).

SIRT3: SIRT3 is expressed in mitochondria and directly regulates important mitochondrial enzymes of the TCA cycle, fatty acid metabolism and ketone synthesis, such as long chain acyl-CoA dehydrogenase (LCAD), Isocitrate dehydrogenase 2 (IDH2), succinate dehydrogenase (SDH), 3-hydroxymethylglutaryl-CoA synthase 2 (HMGCS2) (Finley et al., 2011, Hirschey et al., 2010, Shimazu et al., 2010, Yu et al., 2012). Antioxidant MnSOD function was regulated by SIRT3 through direct deacetylation and promoter deacetylation (Sundaresan et al., 2009, Tseng et al., 2013). In SIRT3 knockout mice, MnSOD activity was decreased due to hyperacetylation, thereby increasing vascular oxidative stress (Tao et al., 2010, Dikalova et al., 2017). In myeloid specific SIRT3 knockout mice, NLRP3 was activated and IL-1β secreted, resulting in perivascular inflammation and fibrosis (Wei et al., 2021). The effect of SIRT3 on NLRP3 in this study was mediated by deacetylation of pyruvate dehydrogenase E1 alpha (PDHA1) (Wei et al., 2021). Upon stimulation with oxLDL, SIRT3 protected macrophages against NLRP3 inflammasome activation, impaired autophagy and the formation of foam cells (Ding et al., 2021, Liu et al., 2018b). Reduced SIRT3 expression in

diabetic patients was also associated with endothelial dysfunction and coronary artery disease (Gong et al., 2022). In a rat model, NMN was protective against ischemia-reperfusion of the heart, mediated by increased SIRT3 expression (Jafari-Azad et al., 2021).

SIRT4: SIRT4 overexpression suppressed nuclear factor-kappa B (NF-κB) pathway and protected endothelial cells from damage induced by oxLDL (Tao et al., 2019).

SIRT5: SIRT5 interacts with multiple mitochondrial enzymes and has an important antioxidant role as it activates NADPH producing enzymes (Zhou et al., 2016).

SIRT6: It was shown that SIRT6 increased the lifespan in mice (Roichman et al., 2021). SIRT6 worked synergistically with SIRT1 to repair DNA damage (Meng et al., 2020). SIRT6 directly activated NAMPT, which was a positive feedback loop (Sociali et al., 2019). It protected smooth muscle cells from senescence and decreased macrophage foam cell formation and reduced the development of atherosclerosis. SIRT6 also activated protective autophagy (Grootaert et al., 2021, Arsiwala et al., 2020, He et al., 2017).

SIRT7: In response to oxLDL, SIRT7 was significantly downregulated in endothelial cells, whereas SIRT7 knockdown promoted proliferation and migration (Zheng et al., 2018).

5.2 Macrophage metabolism

The polarization of macrophages towards a pro- or anti-inflammatory phenotype is closely linked to their metabolism. M1 macrophages are classically activated by toll-like receptor (TLR) agonists/lipopolysaccharides (LPS) and interferon gamma (IFN-γ) stimulation and act pro-inflammatory with major ROS-production. M2 macrophages are activated by interleukin-4/13 (IL-4/IL-13) stimulation and secrete anti-inflammatory cytokines (Sica and Mantovani, 2012). Hyperglycaemia appears to shift the macrophage polarization towards M1 phenotype both *in vitro* and in pre-diabetic humans (Torres-Castro et al., 2016). In M1 macrophages, activation with LPS or oxLDL induces NF-κB, hypoxia-inducible factor 1-alpha (HIF-1-α) induced glucose transporter 1 (GLUT1) expression, hexokinase, and other glycolytic enzymes (Rius et al., 2008). CD36 binding of oxLDL upregulates trafficking of long chain fatty acid to mitochondria, induced ROS production and facilitated NF-kB activation and pro-inflammatory phenotype (Chen et al., 2019).

In pro-inflammatory macrophages, enhanced glycolysis leads to increased NAD+ consumption and the regeneration of NAD+ in TCA cycle is inhibited. Activation of PARPs and CD38 also contribute to increased NAD+ consumption (Minhas et al., 2019, Amici et al., 2018). Covarrubias et al. reported that CD38 expression was responsible for increased NADase activity and was only expressed on M1, but not M2, macrophages (Covarrubias et al., 2020). In a murine model it was shown that *de novo* NAD+ synthesis was required for a homeostatic macrophage phenotype and anti-inflammatory signalling (Minhas et al., 2019).

In general, *de novo* NAD^+ synthesis is located in the liver, whereas the peripheral tissues are dependent on the liver NAD+ production (Liu et al., 2018a). In 2019 however Minhas et al. provided proof for a complete *de novo* synthesis in macrophages (Minhas et al., 2019). Upon *in vitro* LPS stimulation of human macrophages, NAD+ concentration decreased with an associated compensatory induction of *de novo* pathway genes. Only the expression of QPRT, an important enzyme in *de novo* NAD+ synthesis, was reduced (Minhas et al., 2019). The authors concluded that in immune activated macrophages, QPRT activity and *de novo* NAD+ synthesis were the limiting factors for activity of the mitochondrial sirtuin, SIRT3, and mitochondrial function. As such, NAD+ treatment could restore impaired SIRT3 activity (Zhang et al., 2020). The depressed phagocytic function of macrophages was also restored by increased QPRT expression. In human macrophages, QPRT expression significantly declines with aging and as expected, LPS-induced polarization towards a pro-inflammatory M1 phenotype is increased with age. Importantly, this pro-inflammatory phenotype could be reversed in macrophages from older humans by inducing QPRT expression (Minhas et al., 2019). Inhibition of indoleamine 2,3-dioxygenase 1 (IDO1), the first enzyme of the *de novo* pathway, reduced mitochondrial SIRT3 activity in mice or in human macrophages (Minhas et al., 2019). Moreover, it was shown that inhibition of IDO1 in mice increased atherosclerosis and vascular inflammation (Polyzos et al., 2015).

In M2 macrophages, glucose uptake was increased by mammalian target of rapamycin complex 1 (mTORC1) pathway, but predominantly used for TCA cycle (Covarrubias et al., 2016). Unlike in M1 macrophages, TCA-cycle and oxidative

phosphorylation remained intact (Jha et al., 2015). M2 macrophages had increased fatty acid oxidation and oxidative phosphorylation and acted antiatherogenic upon expression of anti-inflammatory cytokines such as IL-10, which suppressed mTOR and reduced GLUT1 translocation (Ip et al., 2017). Experiments in murine cultured macrophages showed that fatty acid oxidation is required for efferocytosis and induced IL-10 production, whereas glycolysis was not needed (Zhang et al., 2019). An intact electron transport chain was necessary to provide NAD+, which is the substrate for SIRT1 mediated anti-inflammatory IL-10 expression (Zhang et al., 2019). In the experimental setting of impaired mitochondrial NAD+ regeneration, treatment with nicotinamide mononucleotide (NMN) was able to rescue IL-10 production (Zhang et al., 2019).

The pentose phosphate pathway, which synthesized nicotinamide adenine dinucleotide phosphate (NADPH) was upregulated in M1 macrophages and downregulated in M2 macrophages (Haschemi et al., 2012). On the one hand, NAPDH was antioxidative and protects macrophages during ROS-production. On the other hand, nitric oxide synthesis was NAPDH dependent, inhibited mitochondrial oxidative phosphorylation and lead to ROS production (Haschemi et al., 2012). It can be concluded that NAD+ is required for macrophage function and that the inhibition of enzymes involved in NAD+ synthesis impairs macrophage function and increases the development of atherosclerosis.

5.3 T cell metabolism

With the action of antigen presenting cells, specific immune cells are recruited to the site. CD4+ T helper cells recognize antigens such as oxLDL, apolipoprotein B-100 (ApoB100) and are activated. Upon activation they proliferate and secrete TNF-α, interleukin-1 beta (IL-1β), IFN-γ (Koltsova et al., 2012, Stemme et al., 1995). The T regulatory cell (Treg) transcription factor Forkhead box P3 (FOXP3) reduced glycolysis and induced oxidative phosphorylation of NADH to NAD+. These changes allowed Treg to maintain function in low oxygen, high lactate inflammatory areas such as atherosclerotic plaques (Angelin et al., 2017, Björnheden et al., 1999). Despite these adaptions, the unfavourable microenvironment significantly induced Treg apoptosis when compared to other T-cells (Amersfoort et al., 2020). Increased

glycolysis, mediated by HIF-1-α, similar to inflammatory macrophages, was required for Th1/Th17 response (Shi et al., 2011, De Rosa et al., 2015). It was shown that Th17 could promote atherosclerosis in $Ldlr^{-/-}$ mice (Li et al., 2008). T effector cells had reduced fatty acid oxidation, oxidative phosphorylation and induced glycolysis, whereas Tregs showed increased fatty acid oxidation (Chang et al., 2013, Berod et al., 2014, Michalek et al., 2011). Both pro-inflammatory and anti-inflammatory phenotypes of T helper cells were dependent on changes in their metabolism (De Rosa et al., 2015, Elkhal et al., 2016). Previous studies have shown that NAD+ induced differentiation of Treg to Th 17 cells. Intravenous injection in mice as well as in vitro exposure of Treg to NAD+ reduced Treg number and suppressed Treg function (Elkhal et al., 2016). Altogether, these data suggest that increased NAD+ levels can reduce Treg cell number and function and cause a differentiation to proatherogenic Th17 cells.

5.4 Endothelial cell metabolism

In endothelial cells, upon exposal to shear stress at predilection sites in the vascular system, HIF-1-α was activated through the NF-κB pathway. Like the effects in pro-inflammatory macrophages and T-cells, it induced glycolysis and inflammatory cytokines in endothelial cells (Feng et al., 2017). Fatty acid oxidation is necessary to maintain integrity and permeability of the endothelial cells. Inhibition of fatty acid oxidation lead to leakage and hyperpermeability (Patella et al., 2015).

5.5 NLRP3 in atherosclerosis

The NLRP3 inflammasome is a protein complex expressed in numerous cell types, which is comprised of NLRP3, apoptosis-associated speck-like protein containing (ASC) with caspase recruitment domain and the effector caspase 1. The complex is formed and activated in response to stimulation with inflammatory signals. NLRP3 inflammasome priming refers to the process by which recognition of DAMPs and pathogen-associated molecular patterns (PAMPs) leads to increased protein expression of different complex parts. At second, the activation by a variety of stimuli such as ROS, binding of microbial components allows caspase-1 to become active (Blevins et al., 2022). Caspase-1 converts pro-IL-1β/IL-18 to active IL-1β/IL-18, which in turn mediates pro-inflammatory effects (Usui et al., 2012, Martinon et al., 2002).

OxLDL binding and formation of intracellular cholesterol crystals were responsible for the activation NLRP3, leading to inflammation and atherosclerosis (Sheedy et al., 2013, Duewell et al., 2010). In Ldlr$^{-/-}$ mice and humans, the expression of NLRP3 and IL-1β in atherosclerotic plaques were significantly increased (Varghese et al., 2016, Zheng et al., 2013, Cheng et al., 2014, Zheng et al., 2014). In contrast, Menu et al. demonstrated that the atherosclerosis progression in Apoe$^{-/-}$ mice occurred independent of NLRP3 (Menu et al., 2011).

5.6 NMN-treatment

NMN is a precursor of NAD+ shown to replenish NAD+ levels in numerous tissues (Yi et al., 2023). In healthy volunteers, the single dose intravenous application of 300 mg NMN proved to be safe and was shown to increased NAMPT expression in blood leukocytes and NAD+ concentration in the blood (Kimura et al., 2022). Dosages of up to 250mg/day for 24 weeks were proven to be safe and increased plasma concentrations of NMN and NAD+ (Yamane et al., 2023, Akasaka et al., 2023).

In mice, the efficacy and safety of much higher doses (e.g. 50-70x) was shown in several studies. Long term (one year) NMN-treatment (300 mg/kg/day) was well tolerated in mice (Mills et al., 2016). NMN suppressed age associated weight gain, increased total oxygen consumption, energy expenditure and physical activity, NAD+ levels in the blood, liver, skeletal muscle and improved plasma lipid profile and insulin sensitivity (Mills et al., 2016). NMN restored reduced NAD+ levels in white adipose tissue (WAT), liver and skeletal muscle in high-fat diet (HFD) induced diabetic mice (Yoshino et al., 2011). In aged murine hearts it was shown that 300 mg/kg/day oral NMN-treatment for 8 weeks increased NAD+ levels and reversed systolic dysfunction (Whitson et al., 2020). In another study the same dosage reversed age associated vascular dysfunction and increased SIRT1 expression (Yoshino et al., 2011). Intraperitoneal injection of 500 mg/kg NMN for 7 or 10 days in female or male mice, respectively, ameliorated glucose intolerance and improved lipid profiles (Yoshino et al., 2011). NMN-treatment reversed the gene expression changes of genes for inflammatory response, oxidative stress and metabolism induced by HFD (Yoshino et al., 2011).

Antiatherogenic effects have been demonstrated for other NAD+ precursors such as NAD+, NA and NAM (Cao et al., 2022, Kuhnast et al., 2013, Zhai et al., 2019). NAM significantly reduced atherosclerosis in Apoe$^{-/-}$ knockout mice (Mendez-Lara et al., 2020). NA was shown to be beneficial both in mice and humans, however it also has direct lipid lowering potential (Kuhnast et al., 2013, Digby et al., 2012). To our knowledge, the effects of NMN on the development of atherosclerosis are currently unknown.

6 Hypothesis

The goal of the current study was to determine the atheroprotective potential of NMN-treatment in the development of atherosclerosis in male WD-fed Ldlr$^{-/-}$ mice. We aim to examine potential *in vivo* effects and molecular pathways influenced by NMN-treatment.

7 Materials and methods

7.1 Mice

All animal experiments were approved by the Federal Ministry of the Republic of Austria for Education, Science and Research, according to the Animal Testing Act2012 (TVG 2012), with permit number 2021.0.615.892. Male B6.129S7-Ldlr<tm1Her>/J, called Ldlr$^{-/-}$ mice were obtained from Jackson Laboratory (Bar Harbor, ME, USA). Mice were group housed (n=2-3/cage) under conventional conditions, with 12-hour dark/light cycle change, 22°C temperature, and food and water accessible *ad libitum*. Enrichment materials were provided; cages, food and water were changed weekly during body weight measurements.

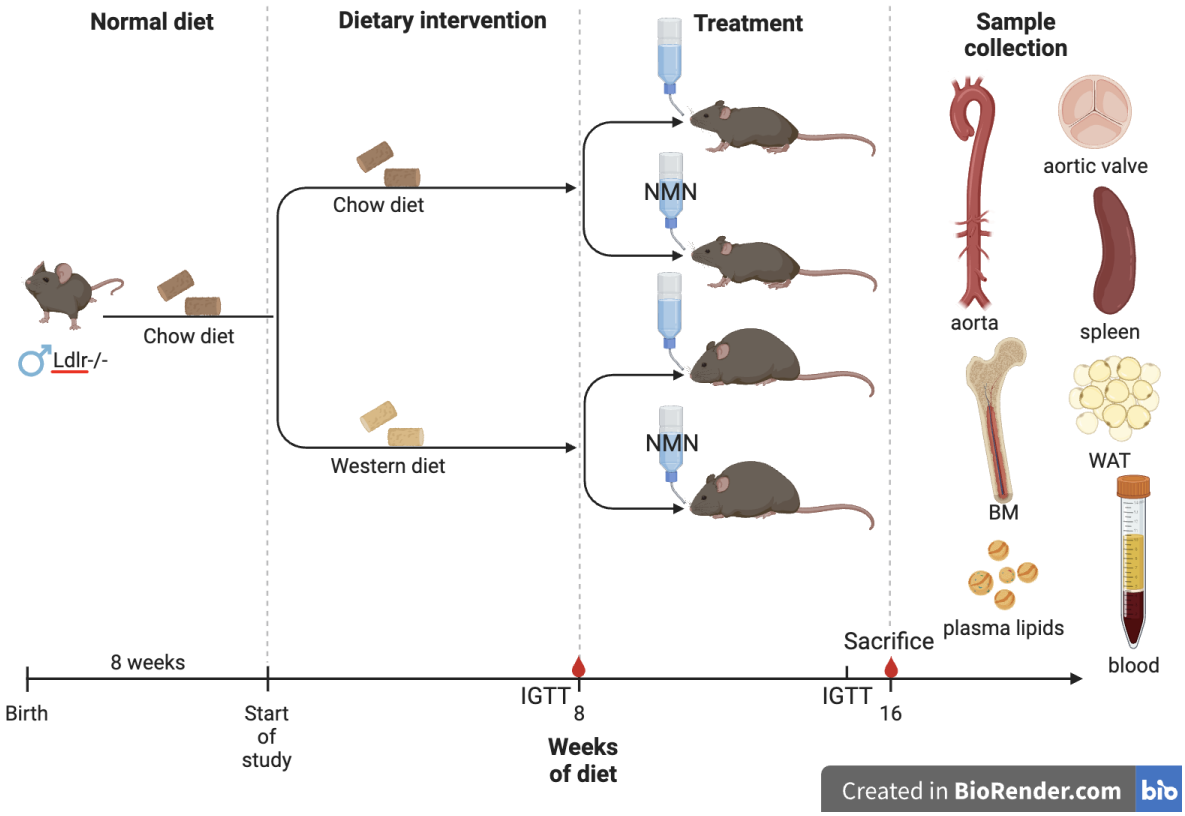

Figure 3: Overview of the study. Male Ldlr-/- mice were fed either a WD or Chow diet, after 8 weeks of diet NMN-treatment in the trinking water was started. The mice were sacrificed after 16 weeks of diet. Created with BioRender.com

7.2 Diet and treatment

Figure 3 provides an overview of the study. 8-week-old male mice weighing 22.84±0.27 g were randomly split into 4 groups: Chow/Vehicle (Veh), WD/Veh, Chow/NMN, WD/NMN (n=6 per group). Chow-fed mice received standard Chow (13.5 MJ/kg, 9 kJ% fat, 24 kJ% protein, 67 kJ% carbohydrates, no cholesterol added, Ssniff Spezialdiäten GmbH # V1534-703, Soest, Germany) and WD-fed mice received a special diet with high-fat and high-cholesterol (metabolizable energy 18.2 MJ/kg, 42 kJ% fat, 19 kJ% protein, 39 kJ% carbohydrates, 1.25 % cholesterol; Ssniff Spezialdiäten GmbH #D12108, Soest, Germany) for 16 weeks, respectively. The special diet was stored cooled and dark, according to the manufacturer's instructions. Fresh diet was provided and food intake was measured weekly. The treatment of the animals was unblinded.

NMN (Oriental Yeast Co. LTD., Tokio, Japan, Lot. 070101) was administered dissolved in drinking water at a dosage of approximately 500 mg/kg/day. The water intake was measured weekly to calculate the required amount of NMN. The NMN-treatment started after 8 weeks of diet and continued for further 8 weeks until the day of dissection after 16 weeks of diet. Since Mills et al. showed that NMN is stable

in water for at least 7 days at room temperature, the water bottles were changed once weekly (Suppl. Figure 1A).

9.3 iGTT measurement

All animals underwent two iGTT at 8 and 15 weeks of diet. Animals were transferred into fresh cages with only bedding material and water without food to fast for 4 hours. A 10 % glucose solution was prepared in 0.9 % saline solution and processed through a sterile filter (Rotilabo KH54.1, Carl Roth GmbH, Karlsruhe, Germany). The bolus dose of 2 g glucose per kg body weight was administered intraperitoneally with a sterile 1 ml syringe and 27G needle. Using a glucometer (Accu-Check Performa, Roche, Mannheim, Germany) the blood glucose measurements were performed immediately before glucose injection and 10, 20, 30, 60, 90 and 120 minutes after injection, using a small drop of blood from a puncture of the tail vein.

7.3 Echocardiography

Echocardiography was performed under isoflurane anaesthesia (Isofluran-Piramal DE9714675, Piramal Critical Care B.V, Voorschoten, Netherlands) after 8 weeks of diet (pre NMN-treatment) and after 16 weeks of diet (post NMN-treatment). Effects of NMN on cardiac function as part of this project were analysed by another student and are not further described in this diploma thesis.

7.4 Blood sampling

Blood (200 µl) was collected 8 weeks and 15 weeks after start of diet as well as during final dissections after 16 weeks of diet (500-1000 µl). Blood was drawn from the retrobulbar plexus with a hemocapillary (Na-heparin minicaps #9411255, Hirschmann, Eberstadt, Germany). Mice underwent isoflurane anaesthesia during the procedure. Blood respectively was collected in a 1.5 ml collection tube containing 5-25 µl 400 mM sodium ethylendiamintetraacetic acid (Na_2-EDTA). Samples were kept on ice until centrifugation at 1000 x g for 10 min at 4°C. Plasma was transferred into a new tube and centrifuged again at 2000 x g for 15 min at 4°C, the supernatant was removed, aliquoted, snap frozen in liquid nitrogen and stored at -80°C for further applications.

7.5 Dissection

Dissections took place after 16 weeks of diet at the age of 24 weeks. Mice underwent isofluran anasthesia followed by blood collection as described in section 9.4. Cervical dislocation was carried out under anaesthesia (confirmed by lack of toe pinch reflex). Dissections were performed under a binocular microscope (M5A, Wild Heerbrugg, Heerbrugg, Switzerland). Beginning with a midline incision, the diaphragm was cut open, remaining blood was drawn from the right ventricle with a 22G needle (Braun, Melsungen, Germany) and the left ventricle was slowly flushed with 5 ml of ice-cold phosphate buffered saline (PBS) (#P4417-100TAD, Sigma-Aldrich, St. Louis, MO, USA) using a 27G needle (Braun, Melsungen, Germany). The heart was cut orthogonal to its length axis, the upper part was used for histology as described in section 9.8. Epididymal fat, left lobe of the liver and kidneys were removed and washed in ice-cold PBS. Organs were finally snap frozen in liquid nitrogen and stored at -80°C for further applications. Spleen and bones were removed and stored in ice-cold PBS for further application. Esophagus, stomach, intestine, lung and trachea were disposed.

The upper third of the heart was pinned down, surrounding tissue of the aorta was removed with fine forceps and microdissection scissors. The aorta was fully exposed from the bulbus aorta until the bifurcation into the iliac arteries, including the supraaortic branches. The arch was detached behind the bulbus aortae, the supraaortic branches at the height of bifurcation of the brachiocephalic artery and right behind the outlet of the left subclavian artery. The thoracic and abdominal aorta was cut right behind the bifurcation into the iliac arteries. Thoracic and abdominal aorta was not separated and is called abdominal aorta throughout this thesis due to simplicity. The abdominal aorta was cut into four equal pieces right after dissection and stored in 300 µl of RNA-later (RNA later #76104, Quiagen, Hilden, Germany).

7.6 Isolation of bone marrow (BM) and spleen-derived leukocytes

For the leukocyte isolation from spleen, a sterile cell strainer (nylon mesh 70 µm #22363548, Thermo Fisher Scientific, Waltham, MA, USA) was wetted with ice-cold PBS and placed on a 20 ml beaker glass (Falcon tubes, Becton, Dickinson and Company, Franklin Lakes, NJ, USA). A 5 ml syringe plunger was used to squeeze

the spleen through the cell strainer, the strainer was flushed through with 10 ml ice-cold PBS. The cell PBS suspension was kept on ice until further processing.
For the leukocyte isolation from bone marrow (BM) both femurs and tibias, the bones were cut at their respective metaphysis. 1-2 ml of ice-cold PBS were flushed through medullary space using a 27G needle, the cell PBS suspension was kept on ice until further processing.
The leukocytes in PBS from BM and spleen were centrifuged with 500 x g for 3 min at 4°C. The pellet was resuspended in 1 ml of ice-cold red blood cell lysis buffer (RBC lysis buffer) (#420301, Bio Legend, San Diego, CA, USA). After 3-4 min of incubation at room temperature cells were centrifuged at 500 x g for further 5 min at 4°C. The supernatant was disposed and the pellet was resuspended in 2 ml ice-cold PBS. A 10 µl sample was used for cell counting using Trypan blue (Trypan blue solution #T8154, Sigma-Aldrich, St. Louis, MO, USA) and a TC20 counter (#1450102, cell counting slides for TC20 cell counter dual-chamber #1450011, Bio-Rad, Hercules, CA, USA,). The remaining sample was aliquoted and then centrifuged again at 500 x g for 5 min at 4°C. The PBS was removed and one aliquot of leukocytes was used fresh for NAD+ measurements while the other aliquots were immediately snap frozen in liquid nitrogen to store them at 80°C for further experiments.

7.7 Histology

After dissection, the upper third of the heart and the arch were embedded in cryomolds (#4566, Sakura Tissue-Tek, Tokyo, Japan) with optimal cutting temperature (OCT) compound (Tissue Plus OCT compound #4586, Scigen Scientific, Gardena, CA, USA), fast frozen on a metal plate on dry ice, frozen at -20°C for 3-4 hours, and transferred to -80°C for long term storage. Before cryotome sectioning, OCT samples were stored at -20°C for 30 min. Cryotome sectioning was performed with a blade temperature of -20°C, object temperature -17°C and chosen thickness of 4 µm (Cryostat microm cryo star HM 560, Thermo Fisher Scientific, Waltham, MA, USA). In relation to the anatomical situs, the heart was cut upside down. As soon as all three leaflets were visible at an equal size, slices were transferred to microscope slides (Superfrost plus microscope slides (J1800 AMNZ), Thermo Fisher Scientific, Waltham, MA, USA).

The aortic arch was processed under the same settings as the heart. The arch was cut longitudinally as soon as full contours of the arch and at least 2 out of three supraaortic branches were completely appeared. The slices were transferred to microscope slides. Both in heart and arch, 10 slides per sample with 3 slices per slide were used, with an ongoing slide organisation to ensure comparability between slides. Slides were dried at room temperature and stored in plastic foil at -80°C until staining.

7.7.1 Oil red O staining (ORO)

Oil red O is a fat-soluble dye which stains lipids red. Thus it can be used to quantify the extent of atherosclerosis. A 0.5 % Oil red O solution (ORO #O0625-25G, Sigma Aldrich dissolved in propylene glycol #0340.2, Carl Roth, Karlsruhe, Germany) was heated at 60°C for 30 min. Frozen sections were dried at room temperature. Slides from each group and region (root and arch) were stained in the same rack, at the same time to ensure comparability. Slides were first fixed in 10 % formalin buffered in PBS (formaldehyde solution with 37 % v/v in H_2O, #252549, Sigma Aldrich, St. Louis, MO, USA) for 10 min, rinsed under tap water for 10 min and submerged in 100 % propylene for 2 min. After fixation, slices were incubated in Oil red O solution for 25 min at 60°C and stained in Hematoxylin solution (Carl Roth, Karlsruhe, Germany) for 2 min. After the staining, the slides were rinsed for 10 min under tap water. Heated glycerol gelatine (GG1, Sigma Aldrich, St. Louis, MO, USA) was used as a mounting media for the cover slips (#1872, Carl Roth, Karlsruhe, Germany). The next day, edges of the coverslips were sealed with nail polish.

7.7.2 Imaging

Imaging was performed using a microscope (Olympus BX 51 with Olympus DP71 Camera system, Tokyo, Japan) analyzed with Cellsens software. The aortic arch and root were imaged using the 4x and 10x objective, respectively. In the case where the aortic root could not be completely covered using 10x objective, the 4x objective was used. The camera filters settings were set to ISO 400 and exposure time 250 ms. The brightest white area was used for white balance. The image files were saved as .png data files for further analysis and randomized for quantification. The analysis was performed blinded to treatment groups.

Image J version 2.1.0 was used for quantification. The images were calibrated to scale bar, the area of annulus fibrosus of the aortic valve and the area of the arch

including the supraaortic branches were encircled. Inside the encircled area, the fraction of red stained area was measured by thresholding method. The following settings were used: hue-saturation-brightness color space, red as threshold color, hue 220-255, saturation 35-255, brightness 100-150, in case of strong staining brightness 70-150. Finally, stained area divided by encircled area was calculated. The results were then unblinded assigned to the groups and analysed according to statistical requirements as described in Section 9.17.

7.8 Cholesterol measurement

Total cholesterol (TC) concentration was measured in plasma using a Cholesterol FS Kit (#113009910021, Diasys, Waterbury, CT, USA). The samples and a standard were diluted 1:5 in 0.9 % NaCl solution according to manufacturer´s instructions. 2 µl of diluted sample, distilled water as blank and diluted standard were pipetted in duplicates into a 96-well plate (Corning Costar 96 well #CLS 3997-50EA, Sigma Aldrich, St. Louis, MO, USA). 200 µl of an assay mix provided as ready to use reagent mix was added to all wells. After 10 min incubation at 37°C the absorbance at 500 nm was measured in a 96-well Spectra Max Plus photometer (Molecular Devices, San Jose, CA, USA). Blank values were subtracted from all values. TC concentrations were calculated according to the standard values and the dilution factor.

7.9 Free fatty acid measurement

The free fatty acid (FFA) concentration was measured in plasma using a Free Fatty Acid Assay Kit (#MAK044-1KT, Sigma Aldrich, St. Louis, MO, USA). The reagents were prepared according to manufacturer´s instructions. The standard series consisted of 0, 2, 4, 6, 8 µl of 1 nmole/µl palmitic acid standard solution. Samples were diluted 1:7 to a final volume of 50 µl in fatty acid assay buffer. Standards and samples were pipetted in duplicates. 2 µl of Acyl-CoA Synthetase reagent was added to each well. Samples and standard were incubated protected from light for 30 min at 37°C. 50 µl master mix consists of 44 µl Fatty Acid Assay Buffer, 2 µl Fatty Acid Probe, 2 µl Enzyme Mix and 2 µl Enhancer was added to each well and the plate was incubated again protected from light for 30 min at 37°C. The absorbance at 570 nm was measured in a 96-well spectra Max Plus photometer. FFA

concentrations were calculated according to the standard values and the dilution factor.

7.10 Triglyceride measurement

Triglyceride (TG) concentration was measured in plasma using Serum Triglyceride Determination Kit (#TR0100, Sigma Aldrich, St. Louis, MO, USA). 3 µl of water for blank, 3 µl of 1mM standard and 3 µl plasma per well were used in a 96-well plate. 80 µl of Free glycerol reagent and 20 µl of TG reagent were added to each well and the plate was incubated at 37°C for 10 min. The absorbance at 540 nm was measured in a 96-well spectra Max Plus photometer. TG concentrations were calculated according to the standard values and the dilution factor.

7.11 NAD+ measurement

Cell pellets of fresh isolated leukocytes as described in Section 9.7 were used for NAD+ measurements using an EnzyChromTM NAD+/NADH Assay Kit ((E2ND-100), EnzyChromTM, BioAssay Systems, Hayward, CA, USA). 100 µl NAD extraction buffer was added to approximately $1x10^7$ cells and cells were resuspended carefully. Homogenization was performed using a tissue grinder (Pellet Mixer Hand-held homogenizer, #47747-370, VWR, Radnor, PA, USA) at maximum speed for 30 seconds. Samples were heated to 60°C for 5 min (Thermomixer comfort, Eppendorf, Hamburg, Germany). A standard curve with a final concentration of 0, 1, 3, 6 and 10 µM NAD+ was prepared. 20 µl assay buffer and 100 µl NADH extraction buffer (to neutralize the reaction) were added to each sample. After vortexing, sample were centrifuged at maximum speed at 4°C for 5 min. For each well the working reagent was prepared as follows: 60 µl assay buffer, 1 µl enzyme A, 1 µl enzyme B, 14 µl lactate and 14 µl MTT were mixed carefully. 80 µl of standard or sample were pipetted in duplicates in a 96-well plate, followed by 80 µl of the prepared working reagent. Absorbance was measured at 565 nm (OD0) using a Spectra Max Plus 96 photometer. After incubation for 15 min at room temperature the absorbance was measured again at 565 nm (OD15). NAD+ concentration was calculated according to the following formula:

$$\textbf{[NAD(H)]}\ (\mu M) = \frac{(OD_{15} - OD_0)_{sample} - (OD_{15} - OD_0)_{blank}}{Slope}$$

NAD+ concentration was normalized to cells counts (µM / 10^7 cells).

7.12 Protein expression measurements

7.12.1 Protein extraction

Frozen leukocytes isolated from spleen as described in Section 9.6, were used for protein isolation. 1–3*10^7 cells per sample were resuspended in 600-1000 µl of ice-cold RIPA buffer (see Table 1) and incubated on ice for 20 min (shaker 20 rpm). The samples were sonicated (UltraSonic Processor UP50H, Amplitude 80%) for 3 seconds on ice and centrifuged at 16,000 x g for 20 - 30 min at 4°C. The supernatant was transferred into an Amicon filter spin column (AMICONULTRA, #UFC51024) and centrifuged in 5 minutes steps at 8,000 x g at 4°C until volume was reduced to 100 µl.

Table 1 RIPA-buffer

	Volume	Final concentration	
Tris-HCL (pH 8) 1.0 M	0.5 ml	50 mM	
EDTA (pH 8) 0,1 M	0.1 ml	1 mM	
NaCl (5 M)	0.3 ml	150 mM	
Igepal (NP40 / CA-630)	0.1 ml	1 %	
Na-deoxycholate 10 %	0.5 ml	0,5 %	
SDS 10 %	0.1 ml	0,1 %	
ddH_20	Up to 10 ml		
Protease inhibitor-cocktail	1 Pill		(#11836153001), Roche, Mannheim, Germany
100 X Phosphatase inhibitor cocktail 2	100 µl		(#P5726), Sigma Aldrich, St. Louis, MO, USA
100 X Phosphatase inhibitor cocktail 3	100 µl		(#P0044), Sigma Aldrich, St. Louis, MO, USA

7.12.2 Protein measurement

The protein concentration was measured using a BCA Protein Assay. 10 µl of 1:4 diluted sample were pipetted in duplicates into a 96-well plate. The standard curve was prepared with serial dilutions of BSA with concentrations of 0.25 mg/ml to 2 mg/ml. To each well 190 µl BCA Protein Assay Mix was added with a ratio of 196 µl reagent A (#23228, Thermo Fisher Scientific, Waltham, MA, USA) and 4 µl reagent B (#23224, Thermo Fisher Scientific, Waltham, MA, USA). The plate was

incubated for 15 min at room temperature. The absorbance at 562 nm was measured in a 96-well Spectra Max Plus photometer. Sample protein concentrations were calculated according to the standard values and the dilution factor.

7.12.3 Automated Western Blot Jess System

When using the Automated Western Blot JESS System protein samples are separated in a very thin matrix gel coated capillary with a total volume of only 10 µl, which allows to determinate protein expression in very small sample quantities compared to the conventional Western Blot technique. Protein expression of SIRT3, NAMPT and acetylated-MnSOD in spleen leukocytes was investigated using these JESS simple Western Blot method according to the manufacturer protocol with following adaptions: Total protein per capillary was 2.4 µg spleen leukocytes protein lysate. An overview of the layout of one JESS plate, which contains samples volume, blocking and washing solutions, primary antibody and secondary antibody dilutions is shown in Figure 4, which was kindly provided by Sartorius AG (Göttingen, Germany). All primary antibodies and corresponding dilutions are listed in Table 2. Alpha-tubulin was used as loading control.

Table 2 Jess Western Blot

Antibody / Target Protein	Dilution and Company
SIRT3	1:10 dilution, (#5490), Cell Signaling Technologies, Danvers, MA, USA
Ac-MnSOD	1:10 dilution, (ab137037), Abcam, Cambridge, UK
NAMPT/PBEF	1:20 dilution, (A300-372A), Thermo Fisher Scientific, Waltham, MA, USA
Alpha-tubulin	1:10 dilution, (#2144), Cell Signaling Technology Danvers, MA, USA

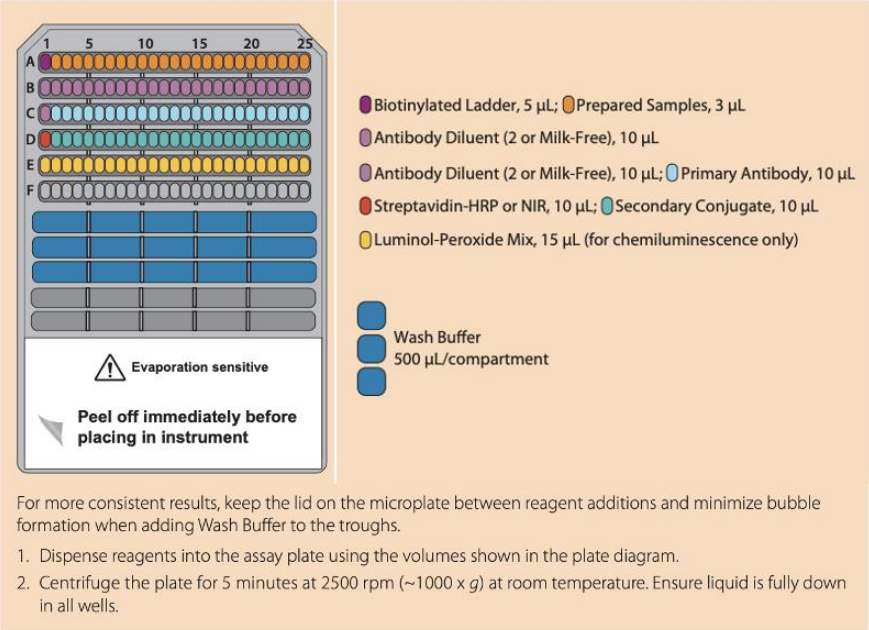

Figure 4: Pipetting template Jess Western Blot from company manual.

7.13 Gene expression experiments

7.13.1 RNA extraction

RNA extraction for the quantitative reverse transcription polymerase chain reaction (RT-qPCR) was performed using a RNeasy Mini Kit (#74104/74106 Quiagen, Hilden, Germany). Frozen cell pellets from spleen leukocytes and bone marrow (BM) were resuspended in RLT lysis buffer containing 1 % 2-Mercaptoethanol (#161-0710, Bio-Rad, Hercules, CA, USA). 350 µl RLT ≤ 5 x 10^6 or 600 µl RLT ≥ 5 x 10^6 cells was used. The suspensions were homogenized for 15-20 sec using an UltraTurrax T10 Homogenizer (IKA, Staufen, Germany) with speed 3 on ice. Samples were then proceeded according to the manufacturing instructions. A RNase-free on-column DNA digest was performed using RNase-free DNase Set (#79254, Quiagen, Hilden, Germany) according to the manufacturing instructions. The RNA concentration was measured using a Nanodrop 2000 spectrophotometer (Thermo Fisher Scientific, Waltham, MA, USA). The samples were frozen in liquid nitrogen and stored at -80°C.

7.13.2 cDNA synthesis (Reverse Transcription – RT)

The complementary single strand deoxyribonucleic acid (cDNA) synthesis was done using a QuantiTect Rerverse Transcription Kit (#205313, Quiagen, Hilden, Germany). The calculated RNA was 500 ng in a total volume of 12 µl. A reverse

transcriptase negative control, called RT minus, consisted of a mixture of several RNA samples from all groups, thereby allows to test for contaminating DNA. 2 µl DNA wipe out reagent was added to each sample and RT minus control, incubated at 42°C for 2 min in a thermal cycler (T100 thermal cycler, Bio-Rad, Hercules, CA, USA). Reverse Transcription master mix and RT minus mix, which are summarized in Table 3 were prepared according to the manufacturer's instructions and 6 µl were added to their respective tubes. The cDNA synthesis was carried out at 42°C for 30 min. Finally, synthesized cDNA was incubated at 95°C for 3 min to inactivate the reverse transcriptase. The cDNA can be stored at -80°C.

Table 3 cDNA master mix

RT master mix	µl/rxn
Reverse Transcriptase	1
RT Buffer 5x	4
Primer Mix	1

RT minus mix	µl/rxn
water	1
RT Buffer 5x	4
Primer Mix	1

7.13.3 cDNA dilution

A cDNA standard dilution series was prepared with a mixture of cDNAs from all investigating samples and RNase/DNase-free water in a dilution of 1:20, 1:100, 1:500, 1:2,500 and 1:12,500. Samples and the RT minus were diluted 1:20 in tube strips (PCR SingleCap 8er-Softstrips 0.2 ml colorless #710971, Biozyme, Hessisch Oldendorf, Germany) and as a second negative control RNase free water was introduced at this step. A random cDNA selected as an interplate calibrator cDNA was prepared and diluted 1:20. Exceptionally for *Nlrp3, Il1b, Tnfa* targets a different standard series (1:20, 1:50, 1:100, 1:200, 1:400, 1:800) and a sample dilution of 1:50 was chosen.

7.13.4 RTqPCR

All samples were assayed in triplicates in 384-well plates (Hard-shell PCR plates 384 well, thin wall #HSP3805, Bio-Rad, Hercules, CA, USA). A master mix was prepared per well as followed: 0.5 µl water, 5 µl Fast advanced Master Mix (#4444557, Thermo Fisher Scientific, Waltham, MA, USA) and 0.5 µl of a respective TaqMan assay probe (Table 4). 6 µl of the master mix was added to each well using a multipipette (#0030089618, Eppendorf, Hamburg, Germany) and 4 µl of the

prepared samples dilutions was added using a multichannel pipette (#99001373, Integra, Biebertal, Germany). The PCR plate was sealed with a clear sealing foil (#15036, Thermo Fisher Scientific, Waltham, MA, USA) and spun down in a plate centrifuge for one minute. All TaqMan assay probes (#4331182) were purchased from Thermo Fisher Scientific, Waltham, MA, USA.

Table 4 TaqMan Assay Probes

TaqMan Assay Probe	Probe ID
Nampt	Mm00451938_m1
Parp1	Mm01321084_m1
18s	Mm03928990_g1
Rplp0	Mm00725448_s1
Actb	Mm00607939_s1
Hprt	Mm03024075_m1
Cd38	Mm00483143_m1
Nmnat1	Mm01257929_m1
Nmnat3	Mm00513791_m1
Sirt3	Mm00452131_m1
Nlrp3	Mm00840904_m1
Il1b	Mm00434228_m1
*Tnf*a	Mm00443258_m1

The following protocol for the CFX384 real time PCR system (Bio-Rad, Hercules, CA, USA) was used:

Table 5 RTqPCR

1.	95°C 2 min 20 sec	Denaturation and polymerase activation
2.	95°C 3 sec	Denaturation
3.	60°C 30 sec	Annealing and Extension
4.		Plate read => Go to Step 2, 44x

7.13.5 Quantification

The quantification was performed using the standard curve method. Threshold cycle values higher than 34 were excluded from standard curve calculation. The arithmetic

mean of the triplicates was formed. The accepted standard deviation of the triplicates was ≤ 0.2.

The concentration values of standard in nanogram were transformed into log10 and a linear straight of best fit was calculated. The slope value of the standard curve was used to calculate the efficiency according to the following formula e=10^(-1/slope). An efficiency of 90-110% was accepted. Since the standard consists of equal amounts of cDNA of all samples no additional efficiency correction is needed to be applied.

The arithmetic mean of the Cq triplicates from Bio-Rad CFX Manager Software was calculated for each sample. According to the slope of the standard regression the mRNA levels have been calculated. The results were expressed relatively to the reference genes results. The results were finally normalized to the Chow/Veh group.

7.13.6 Reference genes

The selection of a suitable reference gene defines the reliability of the results. Important for the selection of a suitable reference gene is a stable expression in all treatment groups. Potential differentially expressed genes were excluded from the search for appropriate reference genes. Two ribosomal coding genes, the cytoplasmic small subunit *18S rRNA* and ribosomal protein lateral stalk subunit P0 (*Rplp0*) as well as the highly conserved structural gene beta-actin *(Actb*) and the purine salvage pathway gene hypoxanthine phosphoribosyltranferase 1 *(Hprt)* have been tested. The expression of the four reference genes was tested in all four experimental groups in BM and spleen leukocytes. Only *Rplp0* was equally expressed in all groups, showed an acceptable amplification efficiency between 90 and 110 % with decent Cq values lower than 34 in its dilution series and, therefore, was selected as the only reference.

7.14 Statistics

Graphpad Prism 10.1.0 and Microsoft Excel version 16.75 were used for all analysis and graphs. All data are presented as mean ± standard error of the mean (SEM). Unpaired t-tests were used for the comparison of two groups. The comparison of four groups was performed with a two-way analysis of variance (2-way ANOVA). A significant diet or treatment effect was shown by symbols & and #, respectively. A

significant interaction term was marked by symbol §. A Shapiro-Wilk and Kolmogorov Smirnov test was used to check for normal distribution. A Tukey's was used as a post-hoc test. A p value ≤ 0.05 was considered as significant.

8 Results

8.1 NMN had no effect on adiposity and glucose tolerance in WD-fed Ldlr$^{-/-}$ mice.

In order to assess the effect of NMN-treatment in atherosclerosis development, we fed Ldlr$^{-/-}$ mice chow or WD for 16 weeks and provided them with standard water or water containing NMN (500 mg/kg/day) in the final 8 weeks of feeding. The 4 different treatment groups were as follows: Chow/Veh, WD/Veh, and Chow/NMN, WD/NMN (n=6).

In order to determine the physiological effects of NMN on characteristic of metabolic syndrome (obesity, glucose intolerance, dyslipidemia, hypertension) (Cornier et al., 2008), we monitored body weight, food intake and performed iGTTs before and after starting NMN-treatment. There was no difference in starting body weight between Chow and WD groups (22.46±0.84 g versus 22.22±0.79 g). However, after 16 weeks of feeding, WD mice gained significantly more body weight compared to Chow mice (35.12±2.00 g in WD/Veh versus 28.46±0.659 g in Chow/Veh; p=0.0133) (Fig. 5A-B). Nevertheless, there was no difference in body weight following NMN-treatment in either Chow- or WD-fed mice (Fig. 5A-B). The caloric intake per mouse was not significantly different between Chow and WD or following NMN-treatment (Supp. fig. 1B), suggesting that NMN did not affect caloric intake. Moreover, adiposity, as shown by WAT mass, was significantly increased by WD; however, there was no effect by NMN-treatment (Fig. 5C). WD elevated fasting blood glucose levels after 8 and 15 weeks of diet (Fig. 5E; Supp. fig. 1D) and impaired glucose tolerance compared to Chow group, which was comparable at both 8 and 15 weeks of feeding (Fig. 5D-F; Supp. fig. 1C-E). Importantly, there was no effect of NMN-treatment on fasting blood glucose or glucose tolerance in either Chow or WD groups (Fig. 5D-F). In summary, WD-fed mice developed obesity and impaired glucose tolerance, but NMN-treatment did not affect body weight, caloric intake, glucose tolerance or epididymal fat mass in Chow- or WD-fed Ldlr$^{-/-}$ mice.

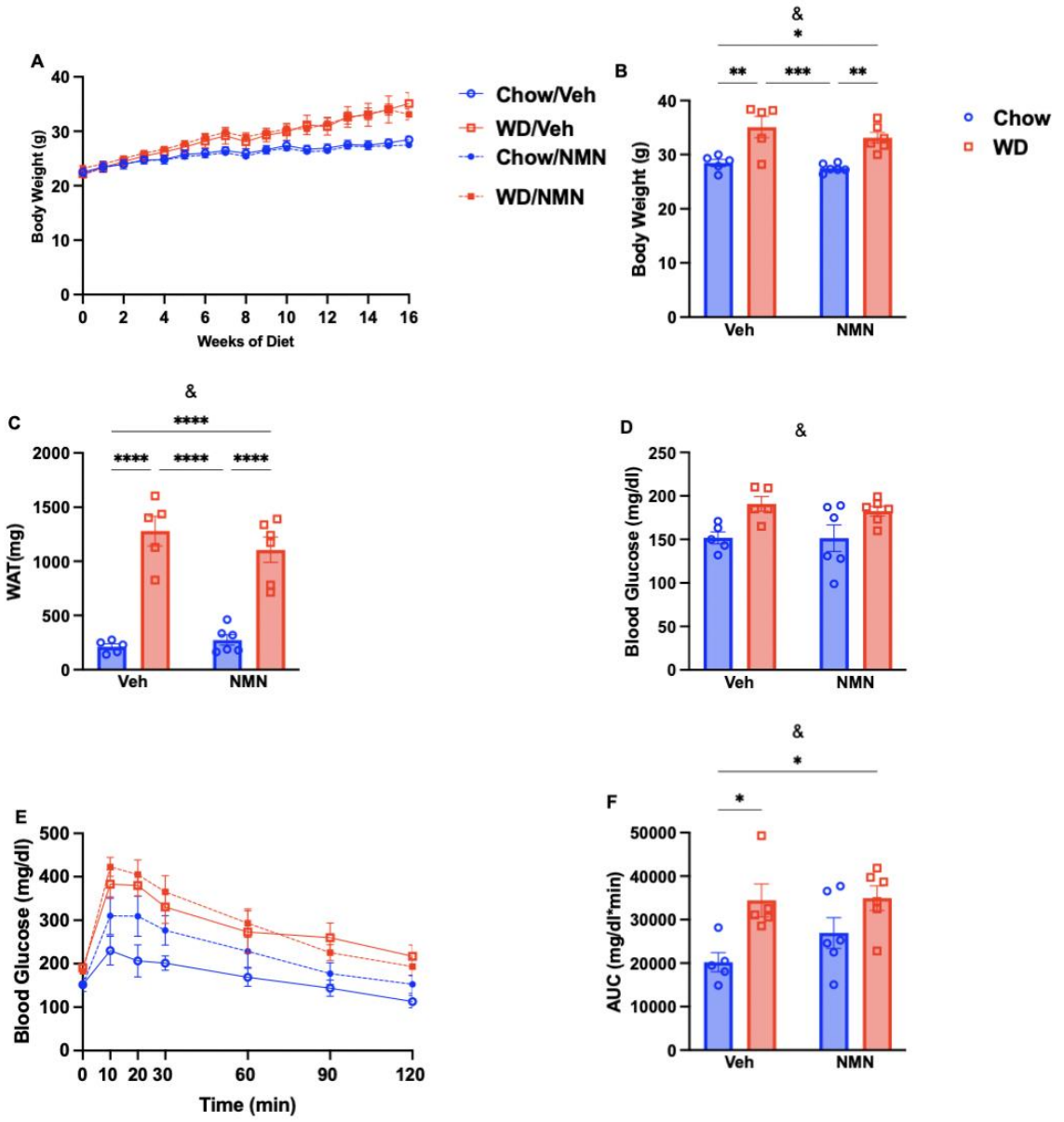

Figure 5: NMN has no effect on body weight, fat mass and glucose tolerance in WD-fed Ldlr-/- mice. A) Body weight, B) body weight after 16 weeks of diet, C) epididymal WAT mass, D) fasting blood glucose, E) iGTT, and F) AUC after 15 weeks of diet in Chow- and WD-fed Ldlr-/- mice treated with Veh or NMN (n=5-6). 2 way-ANOVA: &=effect of diet; ✱ p<0.05, ✱✱✱✱ p<0.0001 using post-hoc test. AUC, area under the curve measured from baseline; iGTT, intraperitoneal glucose tolerance test; Ldlr-/-, low-density lipoprotein receptor knockout; NMN, nicotinamide mononucleotide; WD, western diet; WAT, white adipose tissue.

8.2 NMN-treatment significantly reduced the extent of atherosclerosis in the aortic root of WD-fed Ldlr$^{-/-}$ mice.

To quantify the extent of atherosclerosis, we performed histology with Oil red O staining. WD caused significant lipid deposition in both aortic root and aortic arch compared to Chow-feeding. In the aortic arch, we did not observe any effect of NMN-treatment on the degree of lipid accumulation (Fig 6A-C). However, in the aortic root,

NMN-treatment of WD-fed mice showed a significant reduction of lipid deposition compared to WD/Veh group (Fig. 6B-D). Altogether, NMN-treatment prevented worsening atherosclerotic plaque development in WD-fed $Ldlr^{-/-}$ mice.

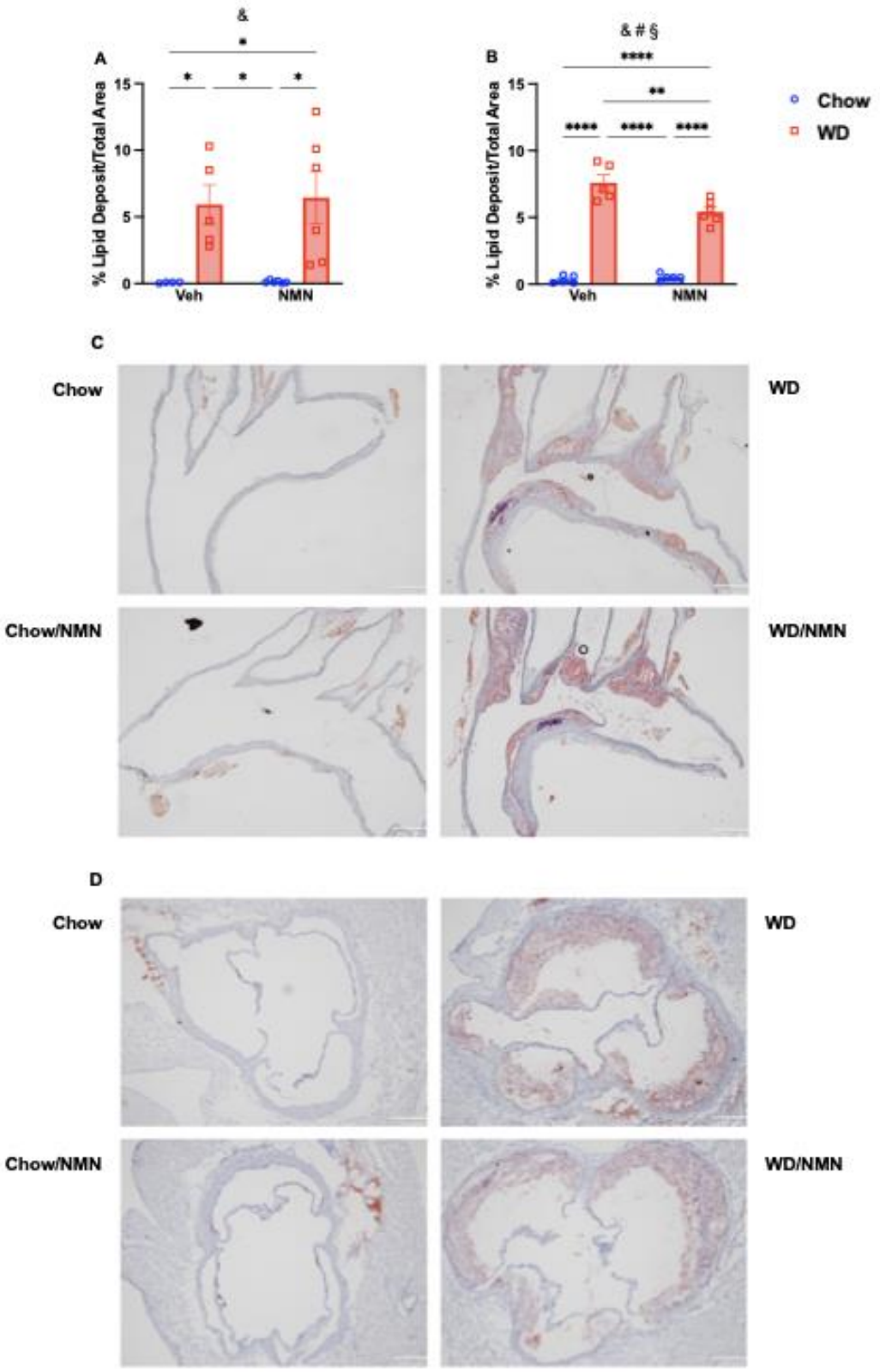

Figure 6: NMN-treatment significantly reduced the extent of atherosclerosis in the aortic root of WD-fed Ldlr-/- mice. Percentage of Oil red O stained lipid deposition of total area aortic A) arch and B) root and representative images of aortic C) arch and D) root in Chow- and WD-fed Ldlr-/- mice treated with Veh or NMN (n=5-6). 2 way-ANOVA: &=effect of diet, #=effect of treatment, §=interaction effect; ✱ p<0.05, ✱✱ p<0.01, ✱✱✱✱ p<0.0001 using post-hoc tests. Ldlr-/-, low-density lipoprotein receptor knockout; Veh, vehicle; NMN, nicotinamide mononucleotide; WD, western diet.

8.3 NMN increases TG with no effect on TC or FFA levels in WD-fed Ldlr$^{-/-}$ mice.

In order to assess NMN effects on plasma lipids, we measured TC, FFA, TG prior and after NMN-treatment. After 8 weeks of diet, WD significantly increased TC, whereas no significant change was observed in TG and FFA levels (Supp. fig. 2A-C). However, after 16 weeks of WD, both TC and TG concentration were significantly increased compared to Chow (Fig 7A-B). NMN had no effect on TC (Fig. 7A), but induced a significantly increased TG concentration in WD-fed mice only (Fig. 7B). After 16 weeks of diet the mean values of FFA levels were equal in all four groups (Fig. 7C). Overall, we show that NMN does not affect WD-induced increase in TC, but further increases TG levels in WD-fed mice.

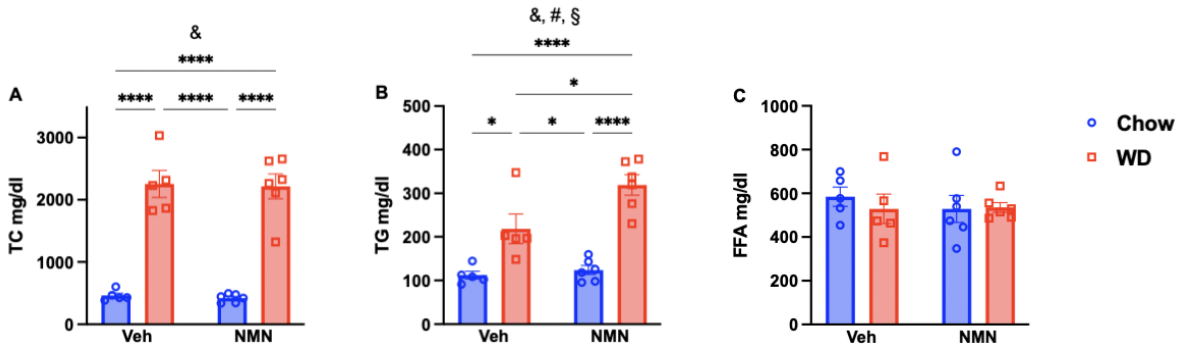

Figure 7: NMN has no effect on TC and FFA levels but significantly increased TG concentrations in WD-fed Ldlr-/- mice. A) TC, B) TG and C) TC concentrations in plasma in Chow- and WD-fed Ldlr-/- mice treated with Veh or NMN (n=5-6). 2 way-ANOVA: &=effect of diet, #=effect of treatment, §=interaction effect; ✱ p<0.05, ✱✱✱✱ p<0.0001 using post-hoc tests. FFA, free fatty acids; Ldlr-/-, low-density lipoprotein receptor knockout; NMN, nicotinamide mononucleotide; TC, total cholesterol; TG, triglycerides; Veh, vehicle; WD, western diet.

8.4 NMN replenished depleted NAD+ levels in leukocytes from WD-fed mice.

In order to investigate how NMN-treatment influences NAD+ levels and production, we performed NAD+ measurements and RT-qPCR for gene expression of key NAD+-producing enzymes *Nampt, Nmnat1,* and *Nmnat3* in leukocytes isolated from spleen and BM. Additionally, we performed automated WB for NAMPT protein expression in leukocytes isolated from spleen. In the BM leukocytes, there was a mild NAD+ depletion in WD/Veh compared to Chow/Veh. Both Chow/NMN and WD/NMN showed mildly elevated NAD+ levels, compared to the respective Veh controls (Fig. 8A). We observed a significant increase in the expression of *Nampt* in BM-derived leukocytes between Chow/NMN and Chow/Veh group (Fig. 8B).

Nmnat1 and *Nmnat3* expression were not significantly different in BM leukocytes (Fig. 8C/D).

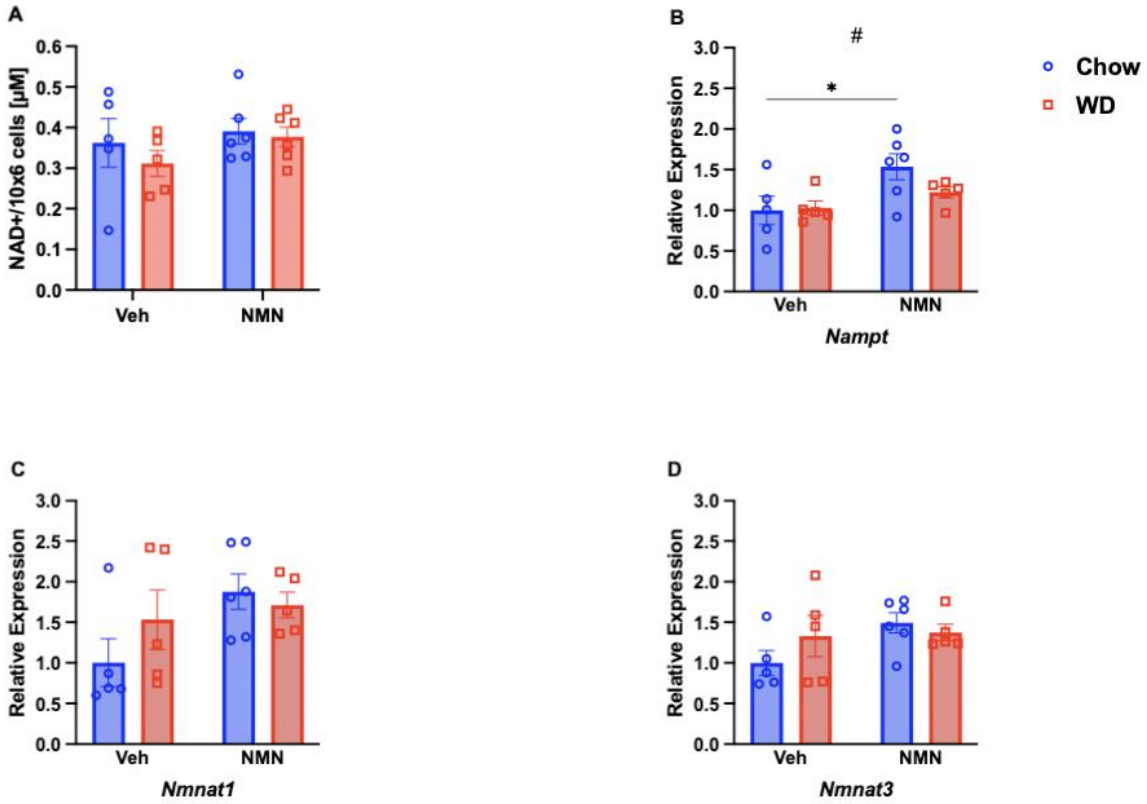

Figure 8: NMN increases Nampt expression in BM-derived leukocytes from Chow-fed mice. A) NAD+ levels and B) Nampt, C) Nmnat1, and D) Nmnat3 gene expression in BM-derived leukocytes of Chow- and WD-fed Ldlr-/- mice treated with Veh or NMN (n=5-6). 2 way-ANOVA: #=effect of treatment; ✱ p<0.05 using post-hoc tests. BM, bone marrow; Ldlr-/-, low-density lipoprotein receptor knockout; Nampt, nicotinamide phosphoribosyl transferase; NMN, nicotinamide mononucleotide; Nmnat1/3, nicotinamide mononucleotide adenylyl transferase 1/3; Veh, vehicle; WD, western diet.

We observed a trend towards reduced NAD+ levels in spleen leukocytes in WD/Veh compared to Chow/Veh (p=0.1884, 2-way-ANOVA diet effect p= 0.0975) (Fig. 9A). NMN-treatment in WD group shows normalization of mean NAD+ levels comparable to Chow/NMN group (Fig. 9A). *Nampt* and *Nmnat1* gene expression were significantly increased in WD/Veh group compared to Chow/Veh. This increase in WD/Veh group was significantly reduced by NMN-treatment (Fig. 9B/C). There were no changes in *Nmnat3* gene expression between any groups (Fig. 9D). Furthermore, we confirmed the significant increase in NAMPT protein expression following WD (Fig. 9E). Our findings in spleen-derived leukocytes suggests that NMN replenishes NAD+ and restores gene expression of NAD+-producing enzymes in WD-fed Ldlr$^{-/-}$ mice.

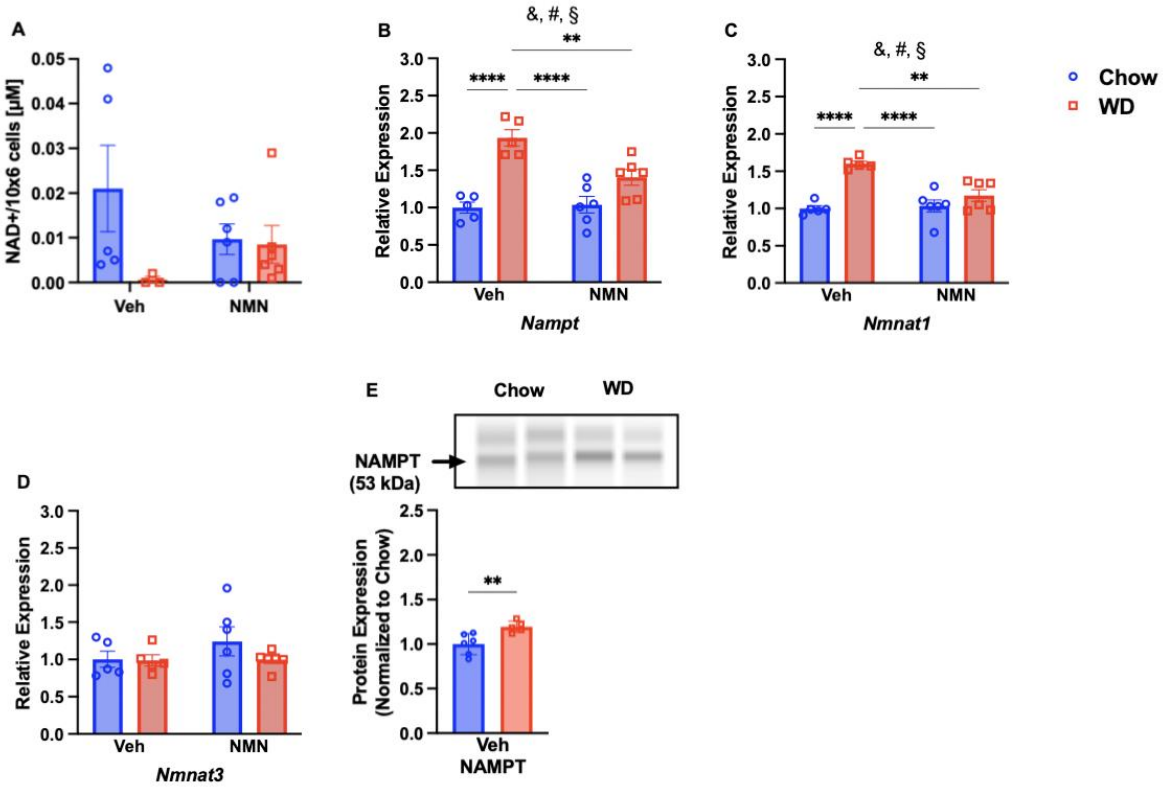

Figure 9: NMN replenishes depleted NAD+ levels and attenuated increased expression of Nampt and Nmnat1 in spleen-derived leukocytes from WD-fed mice. A) NAD+ levels and gene expression of B) Nampt, C) Nmnat1, and D) Nmnat3 and E) protein expression of NAMPT in spleen-leukocytes of Chow- or WD- fed Ldlr-/- mice treated with Veh or NMN (n=5-6). T-test, 2 way-ANOVA: &=effect of diet, #=effect of treatment, §=interaction effect; ✱✱ p<0.01, ✱✱✱✱ p<0.0001 using post-hoc tests. Ldlr-/-, low-density lipoprotein receptor knockout; Nampt, nicotinamide phosphoribosyl transferase; NMN, nicotinamide mononucleotide; Nmnat1/3, nicotinamide mononucleotide adenylyl transferase 1/3; Veh, vehicle; WD western diet.

8.5 NMN normalized the gene expression of *Parp1* and *Cd38* in spleen-derived leukocytes in WD-fed mice.

In order to determine whether leukocyte NAD+ depletion alters expression of NAD+-utilizing enzymes, we measured gene expression of *Parp1, Cd38* and *Sirt3*. In BM-derived leukocytes there were no significant changes in gene expression of *Parp1, Cd38* or *Sirt3* between any groups, although gene expression of *Parp1* and *Cd38* were mildly elevated by WD (Fig. 10A-C).

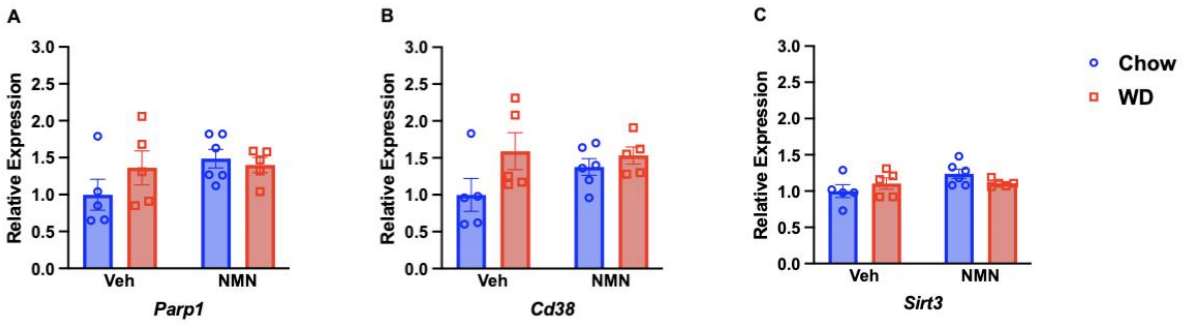

Figure 10: NMN has no effect on expression of NAD+ consuming enzymes Parp1, Sirt3 and Cd38 in BM-derived leukocytes in WD-fed mice. RT-qPCR relative expression, standardized to Chow group, in spleen leukocytes of A) Parp1, B) Cd38 and C) Sirt3 in Chow- and WD-fed Ldlr-/- mice treated with Veh or NMN (n=5-6). 2 way-ANOVA using post-hoc tests. BM, bone marrow; Cd38, cluster of differentiation 38; Ldlr-/-, low-density lipoprotein receptor knockout; NMN, nicotinamide mononucleotide; Parp1, poly ADP-ribose polymerase 1; cyclic ADP ribose hydrolase; Sirt3, Sirtuin 3; Veh, vehice; WD, western diet.

However, in spleen-derived leukocytes, gene expression of *Parp1, Cd38* and *Sirt3* were significantly increased by WD (Fig. 11 A-C). NMN-treatment significantly reversed the increase in gene expression of both *Parp1 and CD38* in WD-fed mice (Fig. 11A-B). Moreover, NMN blunted the increase in *Sirt3* expression induced by WD (Fig. 11C). SIRT3 deacetylates acetylated manganese superoxide dismutase (Ac-MnSOD), which reduces oxidative stress by its superoxide dismutase function (Tao et al., 2010).-Following WD-feeding, there was a significant reduction of SIRT3 protein expression in spleen leukocytes compared to Chow (Fig. 11D). In line with this, we observed significantly increased acetylation of MnSOD in WD- compared to Chow-fed mice (Fig. 11E). Altogether, WD induced increased expression of NAD+-utilizing enzymes and impairs SIRT3 activity in spleen leukocytes and NMN-treatment attenuated the effects of WD on *Parp1* and *Cd38* expression.

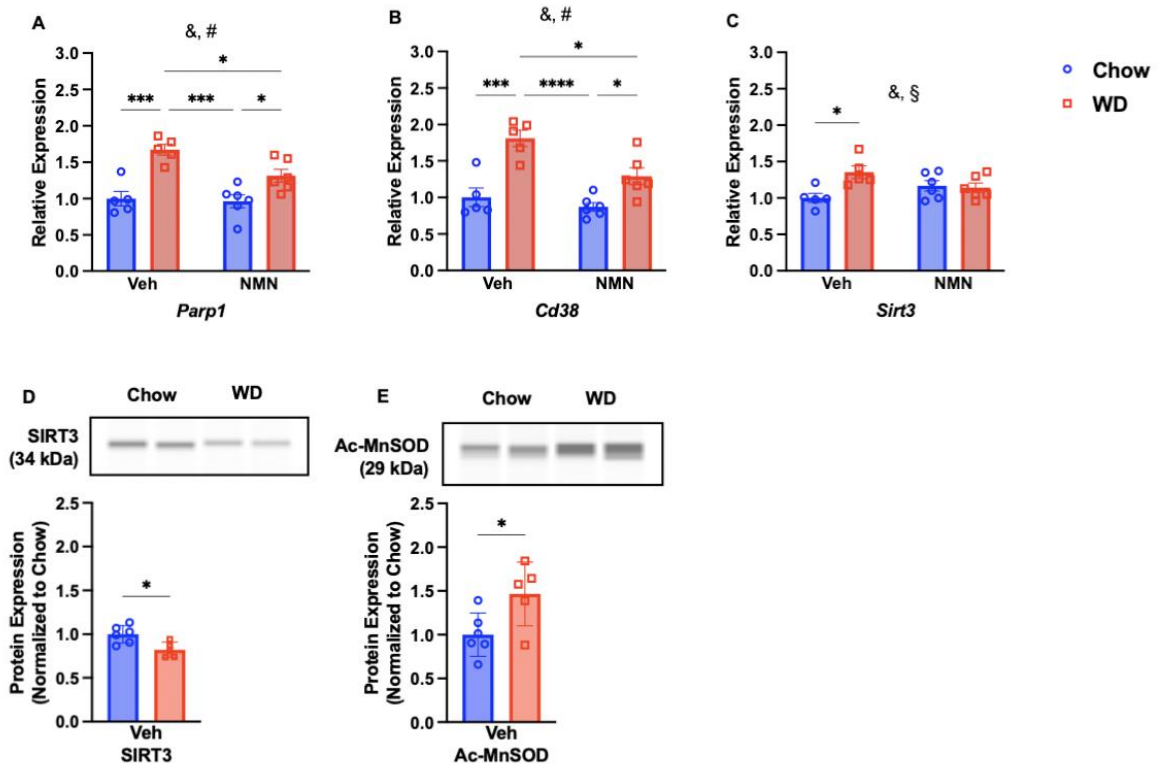

Figure 11: NMN normalized the gene expression of Parp1, Cd38 and Sirt3 in spleen-derived leukocytes in WD-fed mice. Gene expression of A) Parp1, B) Cd38 and C) Sirt3; protein expression of D) SIRT3 and E) Ac-MnSOD in spleen leukocytes of Chow- or WD- fed Ldlr-/- mice treated with Veh or NMN (n=5-6). 2 way-ANOVA: &=effect of diet, #=effect of treatment, §=interaction effect; ✱ p<0.05, ✱✱✱ p<0.001, ✱✱✱✱ p<0.0001 using post-hoc tests. Ac-MnSOD, acetylated manganese superoxide dismutase; Cd38, cluster of differentiation 38, cyclic ADP ribose hydrolase; Ldlr-/-, low-density lipoprotein receptor knockout; NMN, nicotinamide mononucleotide; Parp1, poly ADP-ribose polymerase 1; Sirt3, Sirtuin 3; Veh, vehicle; WD, western diet.

8.6 NMN attenuated the WD-induced increase in gene expression of inflammatory genes in spleen-derived leukocytes.

To get insight into effects of NMN on inflammation, we examined gene expression of *Nlrp3, Il1b,* and *Tnfa* in leukocytes from BM and spleen. NLRP3 is part of the inflammasome and highly involved in the inflammatory response. In BM-derived leukocytes, the expression of *Nlrp3, Il1b,* and *Tnfa* were mildly reduced in the WD/Veh group compared to Chow/Veh (Fig. 12A). Both in Chow and WD group, there were significant increases in *Nlrp3* gene expression upon NMN-treatment (Fig. 12A). The gene expression of *Il1b* and *Tnfa* showed a similar increase upon NMN-treatment (Fig. 12B/C).

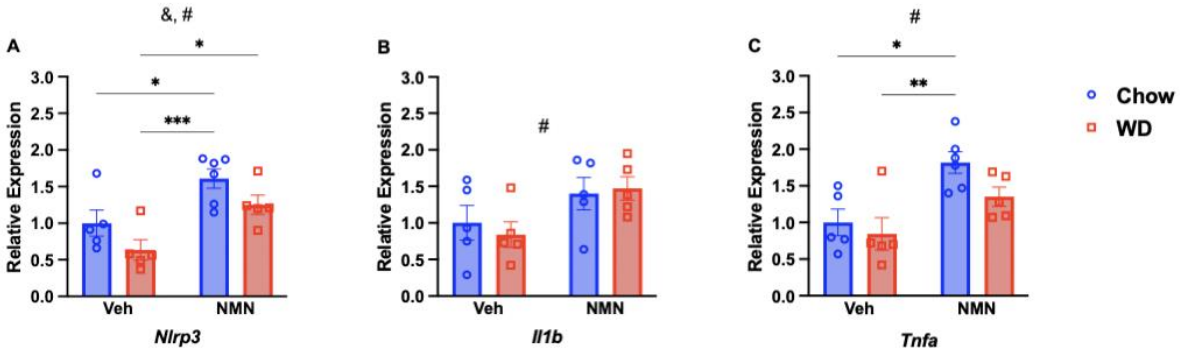

Figure 12: NMN increases gene expression of Nlrp3, Il1b and Tnfa in BM-derived leukocytes from Chow and WD-fed mice. Gene expression of A) Nlrp3, B) Il1b and C) Tnfa in BM leukocytes of Chow- and WD-fed Ldlr-/- mice treated with Veh or NMN (n=5-6). 2 way-ANOVA: &=effect of diet, #=effect of treatment p<0.05; ✱ p<0.05, ✱✱ p<0.01, ✱✱✱ p<0.001, using post-hoc tests. Ldlr-/-, low-density lipoprotein receptor knockout; Il1b, Interleukin-1 beta; Nlrp3, NLR family pyrin domain containing 3; NMN, nicotinamide mononucleotide; Tnfa, tumor necrosis factor alpha; Veh, vehicle; WD, western diet.

In spleen derived leukocytes, gene expression of *Nlrp3, Il1b* and *Tnfa* were increased in WD/Veh compared to Chow/Veh (p=0.3660, 0.1620, 0.1560) (Fig. 13A-C). (Fig. 13A-C). In WD-fed mice the increase in *Nlrp3, Il1b* and *Tnfa* gene expression was attenuated by NMN, a significance was not reached. We observed an overall treatment effect of NMN on *Tnfa* expression (Fig. 13A-C). Altogether, we showed that NMN-treatment reduced the pro-inflammatory changes in spleen derived leukocytes, whereas in BM-derived leukocytes NMN increased the expression of pro-inflammatory genes.

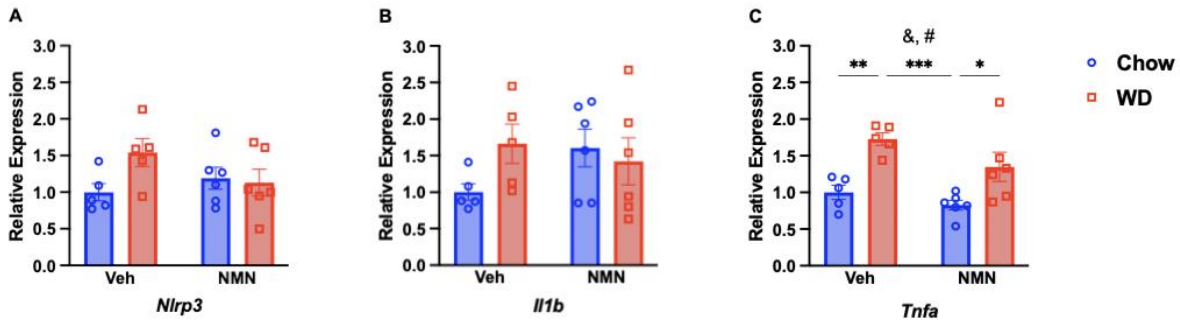

Figure 13**: NMN attenuates the WD-induced increase in gene expression of Nlrp3, Il1b and Tnfa in spleen-derived leukocytes.** Gene expression of A) Nlrp3, B) Il1b and C) Tnfa , in spleen leukocytes of Chow- and WD-fed Ldlr-/- mice treated with Veh or NMN (n=5-6). 2 way-ANOVA: &=effect of diet, #=effect of treatment; ✱ p<0.05, ✱✱ p<0.01, ✱✱✱ p<0.001 using post-hoc tests. Il1b, Interleukin-1 beta; Ldlr-/-, low-density lipoprotein receptor knockout, Nlrp3, NLR family pyrin domain containing 3; NMN, nicotinamide mononucleotide; Tnfa, tumor necrosis factor alpha; Veh, vehicle; WD, western diet.

9 Discussion

9.1 Atherosclerosis

In the current study, we show the effects of NMN-treatment on the development of atherosclerosis in WD-fed male Ldlr$^{-/-}$ mice. We demonstrate for the first time that the development of atherosclerosis is significantly attenuated by NMN-treatment. Previous studies reported that WD with cholesterol and fat content between 0.15-1.25 % and 15-20 %, respectively, significantly increased atherosclerosis after 12-16 weeks of feeding in C57BL/6J Ldlr$^{-/-}$ mice (Lichtman et al., 1999, Teupser et al., 2003). We used a WD containing 1.25 % cholesterol and 20 % of fat which successfully induced distinct atherosclerotic lesions in both the aortic root and aortic arch. Importantly, we showed that NMN significantly reduced atherosclerosis in the aortic root of WD-fed male Ldlr$^{-/-}$ mice. It was previously shown that NMN was protective against vascular dysfunction in aged mice (de Picciotto et al., 2016, Tarantini et al., 2019). The treatment with different NAD+ precursors (NAM, NA) in other mouse models of atherosclerosis (including ApoE$^{-/-}$and Ldlr$^{-/-}$) similarly reduced the development of atherosclerotic plaques (Mendez-Lara et al., 2020, Kuhnast et al., 2013, Abdellatif et al., 2022, Lukasova et al., 2011). However, to the best of our knowledge, this is the first study to demonstrate that NAD+ supplementation using NMN-treatment also reduces the development of atherosclerosis.

9.2 Body weight and adiposity

Our study showed that NMN-treatment did not reduce body weight or adiposity or improve glucose intolerance induced by WD. A study in obese C57BL/6J mice treated with 500 mg/kg/day NMN, the same dosage as in our study but for longer duration (18 weeks), showed decreased adipose tissue mass, increased lean mass, normalized blood lipids and alleviated insulin resistance after NMN-treatment (Zhang et al., 2023). Another study in HFD-fed C57BL/6J mice treated with oral 500mg/kg/day NMN for 8 weeks, reported decreased body weight and subcutaneous fat (Imi et al., 2023). In the light of these studies, we would have expected a beneficial effect of NMN on adiposity and glucose intolerance. As such, NMN may prevent the development of obesity and glucose intolerance, but may be

insufficient to reverse these conditions once already established. Our findings suggest that the atheroprotective effects of NMN occurred independent of improvements in body weight or glucose tolerance.

9.3 Dyslipidaemia

In our study, we did not observe an effect of either WD or NMN on FFA levels in our study. Moreover, TC in plasma was significantly increased by WD, but no effect of NMN was observed. Although TC is considered a risk factor of atherosclerosis, this finding suggests that the atheroprotective effect of NMN is not mediated by a reduction of TC in the current study. Interestingly, we showed that NMN-treatment significantly increased TG levels, beyond that of WD-feeding alone. In contrast to our findings, Yoshino et al. showed in age induced diabetic mice that the levels of TC, TG and FFA were significantly increased with WD and reduced to normal levels after intraperitoneal NMN-treatment for 10 consecutive days (Yoshino et al., 2011). It was also previously shown that NMN decreases TG in humans (Kimura et al., 2022). Furthermore, Imi et al. showed that NMN induced lipolysis by activation of the SIRT1-AMPK axis which activates adipose triglyceride lipase (ATGL) (Imi et al., 2023). ATGL converts TG to FFA, which could explain a reduction in TG levels. However in line with our findings, Yamane et al. reported in 2023 that 12 week long oral 250mg/day NMN-treatment of healthy humans non-significantly elevated TG levels in blood after 8 and 12 weeks of treatment, without providing mechanistic insights into this finding (Yamane et al., 2023). Altogether, we conclude that the atheroprotective effect of NMN was not mediated by reductions in plasma lipids.

9.4 NAD+ synthesis and consumption

In order to determine the role of leukocyte NAD+ in the atheroprotective effects of NMN, we measured NAD+ levels and the expression of genes involved in NAD+-utilization in BM- and spleen-derived leukocytes. In BM- and spleen-derived leukocytes, we observed a mild depletion of NAD+ by WD, which seemed to be reversed by NMN-treatment. We are the first group to report NAD+ depletion in leukocytes in $Ldlr^{-/-}$ mice following WD-feeding. In hypertensive humans, NAD+ depletion in PBMC has been previously shown, without changes in related other metabolites, such as NAM, NR, and NADPH. Thus NAD+ appears to be a suitable

marker for effects of NMN-treatment (Qiu et al., 2023). Previous studies have similarly shown the ability of NMN to replenished NAD+ levels in leukocytes (Kimura et al., 2022). Moreover, Qiu et al. conducted a small-scale clinical trial which showed that that treatment of hypertensive humans with 800 mg NMN/day for 30 days significantly increased NAD+ levels in PBMCs (Qiu et al., 2023). From a translational perspective, this NAD+ repletion in human leukocytes using NMN-treatment combined with our murine *in vivo* results is a promising therapeutic option for the prevention of leukocyte NAD+ depletion in atherosclerosis.

NMNAT enzymes convert NMN to NAD+ and are the second last step of NAD+ *de novo* synthesis and Preiss-Handler pathway. NAMPT, in contrast to NMNATs, is only involved in salvage pathway of NAD+ synthesis and converts NAM to NMN. It was reported that macrophages in human carotid plaques showed distinct expression of NAMPT (Bermudez et al., 2017). PBMCs isolated from diabetic humans were shown to have an increased inflammatory state, reduced NAD+ and a downregulated expression of NAMPT (Alshahrani et al., 2019, de Kreutzenberg et al., 2010). Contrary to that, Bermudez et al. reported that overexpression of NAMPT specifically in leukocytes in $Ldlr^{-/-}$ knockout mice attenuated the development of atherosclerosis, and skewed the inflammatory response towards anti-inflammatory M2 phenotype (Bermudez et al., 2017). However *in vitro* studies showed that NAMPT was significantly upregulated in M1 macrophages and knockout of NAMPT inhibited M1 polarization (Halvorsen et al., 2015, Venter et al., 2014). We wanted to evaluate the role of leukocytes in our model.

Our study showed that NMN-treatment reduced the WD-induced upregulation of *Nampt* and *Nmnat1* in spleen derived leukocytes. This upregulation by WD was in line with the mentioned *in vitro* data. We interpret this upregulation to be compensatory, as NAD+ levels were depleted following WD-feeding. Until now the transcriptional regulation of *Nmnat1/3* is not clear (Fortunato et al., 2022). It is important to note that we only measured *Nampt* gene expression in leukocytes. Pro-inflammatory eNAMPT is located extracellularly and was not measured in the current study. Leukocyte specific overexpression of NAMPT in our $Ldlr^{-/-}$ model would give insights whether the upregulation by WD was compensatory.

After NAD+-producing enzymes, we took a look on NAD+-consuming enzymes. In spleen leukocytes, both *Parp1* and *Cd38* were significantly increased by WD and

NMN-treatment attenuated the increase. It has been shown that CD38 was induced in human macrophages during inflammatory conditions (Amici et al., 2018) and that increased CD38 expression was responsible for the age-dependent NAD+ depletion and mitochondrial dysfunction (Camacho-Pereira et al., 2016). Mitochondrial dysfunction and ROS induced DNA damage which, by itself, increased *Parp1* expression, another consumer of NAD+ (Ke et al., 2019). A such, we believe that increased expression of *Parp1* and *Cd38* in response to WD feeding, may contribute to NAD+ depletion we observe in leukocytes in the current study.

Moreover, we showed that WD-induced NAD+ depletion in leukocytes was associated with impaired SIRT3 protein expression and increased acetylation of its mitochondrial antioxidant target, MnSOD, indicating decreased SIRT3 function. Previous studies have shown that SIRT3 activity is dependent on NAD+ concentration (Houtkooper et al., 2010). Hyperacetylation of MnSOD reduces its SOD activity, resulting in increased ROS (Tao et al., 2010). ROS is responsible for DNA damage; the repair consumes NAD+ through PARP1 and sirtuins. As such, SIRT3 impairment and MnSOD hyperacetylation is associated with vascular oxidative stress in mice (Dikalova et al., 2017). Interestingly, PBMCs from hypertensive humans display reduced *Sirt3* expression and increased acetylation of MnSOD (Dikalova et al., 2017). Altogether, we showed that WD impairs SIRT3 expression and activity. We showed that WD induced NAD+ depletion associated with increased expression of NAD+ consuming enzymes and impaired SIRT3 expression. NMN replenished NAD+ levels and attenuated the increased expression of NAD+ consuming enzymes in WD-fed mice.

9.5 Inflammation

The link between immune cells and atherosclerosis is inflammation (Libby, 2021). In our current study we showed that in spleen-derived leukocytes, WD increased the expression of inflammatory genes (*Nlrp3, Il1b, Tnfa*) and NMN blunted the increase. Whereas in BM-derived leukocytes, WD mildly reduced the expression of these genes and both in Chow and WD group the expression was increased by NMN. Previous studies have shown that NMN exerted anti-inflammatory effects in BM-derived macrophages (Shim et al., 2021). One reason for our contrary finding could be that we did not separate macrophages from other leukocytes, thus a

change in macrophages alone could have been hidden. Shim et al. reported that in BM-derived macrophages, NAD+ depletion led to NLRP3 inflammasome assembly, activation and IL-1β release; effects which were abrogated by NMN-treatment. (Shim et al., 2021). Another study uncovered that NAM, another NAD+ precursor, decreased TNF-α synthesis in macrophages *in vitro* as well as reduced TNF-α in the blood of mice, mediated by sirtuins *(Van Gool et al., 2009).* There was no previous study on the effect of NMN or other precursors on spleen-derived leukocytes. Whether or not NMN also exerts anti-inflammatory effects on circulating leukocytes would be interesting to study in our model as well as in humans. To sum up these findings, we showed that NMN attenuated inflammation in spleen-derived leukocytes of WD-fed mice, but further *in viv*o and *in vitro* studies are needed to uncover the underlying mechanisms.

9.6 Limitations

One major limitation of this study is that only male mice were used. The same experiments are already planned in female mice, as it is well known that the extent of atherosclerotic lesions differs between male and female mice and in humans (Man et al., 2020). Mansukhani showed that female Ldlr$^{-/-}$ knockout mice fed with HFD suffered from more severe hyperlipidemia and atherosclerosis compared to their male counterparts (Mansukhani et al., 2017). It was shown that although plasma NAD+ and NADH levels are not significantly different between men and women, women showed a higher NAD+/NADH level (Yoshino et al., 2021, Igarashi et al., 2022, Yi et al., 2023, Schwarzmann et al., 2021).

Moreover, leukocytes used in this study were not separated in cell subtypes (such as macrophages, cytotoxic or helper T-cells, B cells, etc). Cell sorting would be an important next step to quantify NAD+ levels of these cell subtypes, in order to obtain a better understanding of the effects of NMN in specific immune cell types. Moreover, immunohistochemistry of root and arch for specific leukocyte cell subtypes such as macrophages (CD68, Mac3), T-cells (CD3+, CD4+, CD8+) could provide a better understanding of how leukocyte infiltration is altered upon NMN-treatment following WD-feeding. Finally, single cell RNA sequencing (scRNAseq) of immune cells from the blood, spleen and BM would provide deep insights into novel potential mechanisms involved in atherosclerosis development (Fernandez and

Giannarelli, 2022). This would extend our understanding of the treatment potential of NMN in atherosclerosis.

10 Conclusion

Altogether, we show that NMN treatment attenuated the development of atherosclerosis in a murine model of atherosclerosis, indicating that NAD+ depletion contributes to atherosclerosis pathogenesis, possibly by impairing SIRT3 activity and amplifying NLRP3 activity in leukocytes. Thus, NAD+ supplementation may be a promising strategy to attenuate or prevent development of atherosclerosis.

11 References

ABDELLATIF, M., BUGGER, H., KROEMER, G. & SEDEJ, S. 2022. NAD(+) and Vascular Dysfunction: From Mechanisms to Therapeutic Opportunities. *J Lipid Atheroscler,* 11**,** 111-132.

ABDELLATIF, M., SEDEJ, S. & KROEMER, G. 2021. NAD(+) Metabolism in Cardiac Health, Aging, and Disease. *Circulation,* 144**,** 1795-1817.

AKASAKA, H., NAKAGAMI, H., SUGIMOTO, K., YASUNOBE, Y., MINAMI, T., FUJIMOTO, T., YAMAMOTO, K., HARA, C., SHIRAKI, A., NISHIDA, K., ASANO, K., KANOU, M., YAMANA, K., IMAI, S.-I. & RAKUGI, H. 2023. Effects of nicotinamide mononucleotide on older patients with diabetes and impaired physical performance: A prospective, placebo-controlled, double-blind study. *Geriatrics & Gerontology International,* 23**,** 38-43.

ALLAHVERDIAN, S., CHEHROUDI, A. C., MCMANUS, B. M., ABRAHAM, T. & FRANCIS, G. A. 2014. Contribution of Intimal Smooth Muscle Cells to Cholesterol Accumulation and Macrophage-Like Cells in Human Atherosclerosis. *Circulation,* 129**,** 1551-1559.

ALSHAHRANI, A., ALDUBAYEE, M., ZAHRA, M., ALSEBAYEL, F. M., ALAMMARI, N., ALSUDAIRY, F., ALMAJED, M. & ALJADA, A. 2019. Differential Expression of Human N-Alpha-Acetyltransferase 40 (hNAA40), Nicotinamide Phosphoribosyltransferase (NAMPT) and Sirtuin-1 (SIRT-1) Pathway in Obesity and T2DM: Modulation by Metformin and Macronutrient Intake. *Diabetes Metab Syndr Obes,* 12**,** 2765-2774.

AMERSFOORT, J., SCHAFTENAAR, F. H., DOUNA, H., VAN SANTBRINK, P. J., VAN PUIJVELDE, G. H. M., SLÜTTER, B., FOKS, A. C., HARMS, A., MORENO-GORDALIZA, E., WANG, Y., HANKEMEIER, T., BOT, I., CHI, H. & KUIPER, J. 2020. Diet-induced dyslipidemia induces metabolic and migratory adaptations in regulatory T cells. *Cardiovascular Research,* 117**,** 1309-1324.

AMICI, S. A., YOUNG, N. A., NARVAEZ-MIRANDA, J., JABLONSKI, K. A., ARCOS, J., ROSAS, L., PAPENFUSS, T. L., TORRELLES, J. B., JARJOUR, W. N. & GUERAU-DE-ARELLANO, M. 2018. CD38 Is Robustly Induced in Human Macrophages and Monocytes in Inflammatory Conditions. *Front Immunol,* 9**,** 1593.

AMJAD, S., NISAR, S., BHAT, A. A., SHAH, A. R., FRENNEAUX, M. P., FAKHRO, K., HARIS, M., REDDY, R., PATAY, Z., BAUR, J. & BAGGA, P. 2021. Role of NAD(+) in regulating cellular and metabolic signaling pathways. *Mol Metab,* 49**,** 101195.

ANGELIN, A., GIL-DE-GÓMEZ, L., DAHIYA, S., JIAO, J., GUO, L., LEVINE, M. H., WANG, Z., QUINN, W. J., 3RD, KOPINSKI, P. K., WANG, L., AKIMOVA, T., LIU, Y., BHATTI, T. R., HAN, R., LASKIN, B. L., BAUR, J. A., BLAIR, I. A., WALLACE, D. C., HANCOCK, W. W. & BEIER, U. H. 2017. Foxp3 Reprograms T Cell Metabolism to Function in Low-Glucose, High-Lactate Environments. *Cell Metab,* 25**,** 1282-1293.e7.

ARSIWALA, T., PAHLA, J., VAN TITS, L. J., BISCEGLIE, L., GAUL, D. S., COSTANTINO, S., MIRANDA, M. X., NUSSBAUM, K., STIVALA, S., BLYSZCZUK, P., WEBER, J., TAILLEUX, A., STEIN, S., PANENI, F., BEER, J. H., GRETER, M., BECHER, B., MOSTOSLAVSKY, R., ERIKSSON, U.,

STAELS, B., AUWERX, J., HOTTIGER, M. O., LÜSCHER, T. F. & MATTER, C. M. 2020. Sirt6 deletion in bone marrow-derived cells increases atherosclerosis - Central role of macrophage scavenger receptor 1. *J Mol Cell Cardiol,* 139**,** 24-32.

BERMUDEZ, B., DAHL, T. B., MEDINA, I., GROENEWEG, M., HOLM, S., PAZ, S. M.-D. L., ROUSCH, M., OTTEN, J., HERIAS, V., VARELA, L. M., RANHEIM, T., YNDESTAD, A., ORTEGA-GOMEZ, A., ABIA, R., NAGY, L., AUKRUST, P., MURIANA, F. J. G., HALVORSEN, B. & BIESSEN, E. A. L. 2017. Leukocyte Overexpression of Intracellular NAMPT Attenuates Atherosclerosis by Regulating PPARγ-Dependent Monocyte Differentiation and Function. *Arteriosclerosis, Thrombosis, and Vascular Biology,* 37**,** 1157-1167.

BEROD, L., FRIEDRICH, C., NANDAN, A., FREITAG, J., HAGEMANN, S., HARMROLFS, K., SANDOUK, A., HESSE, C., CASTRO, C. N., BÄHRE, H., TSCHIRNER, S. K., GORINSKI, N., GOHMERT, M., MAYER, C. T., HUEHN, J., PONIMASKIN, E., ABRAHAM, W.-R., MÜLLER, R., LOCHNER, M. & SPARWASSER, T. 2014. De novo fatty acid synthesis controls the fate between regulatory T and T helper 17 cells. *Nature Medicine,* 20**,** 1327-1333.

BJÖRNHEDEN, T., LEVIN, M., EVALDSSON, M. & WIKLUND, O. 1999. Evidence of hypoxic areas within the arterial wall in vivo. *Arterioscler Thromb Vasc Biol,* 19**,** 870-6.

BLEVINS, H. M., XU, Y., BIBY, S. & ZHANG, S. 2022. The NLRP3 Inflammasome Pathway: A Review of Mechanisms and Inhibitors for the Treatment of Inflammatory Diseases. *Front Aging Neurosci,* 14**,** 879021.

BRUNET, A., SWEENEY, L. B., STURGILL, J. F., CHUA, K. F., GREER, P. L., LIN, Y., TRAN, H., ROSS, S. E., MOSTOSLAVSKY, R., COHEN, H. Y., HU, L. S., CHENG, H. L., JEDRYCHOWSKI, M. P., GYGI, S. P., SINCLAIR, D. A., ALT, F. W. & GREENBERG, M. E. 2004. Stress-dependent regulation of FOXO transcription factors by the SIRT1 deacetylase. *Science,* 303**,** 2011-5.

BRUZZONE, S., FRUSCIONE, F., MORANDO, S., FERRANDO, T., POGGI, A., GARUTI, A., D'URSO, A., SELMO, M., BENVENUTO, F., CEA, M., ZOPPOLI, G., MORAN, E., SONCINI, D., BALLESTRERO, A., SORDAT, B., PATRONE, F., MOSTOSLAVSKY, R., UCCELLI, A. & NENCIONI, A. 2009. Catastrophic NAD+ depletion in activated T lymphocytes through Nampt inhibition reduces demyelination and disability in EAE. *PLoS One,* 4**,** e7897.

BUSSO, N., KARABABA, M., NOBILE, M., ROLAZ, A., VAN GOOL, F., GALLI, M., LEO, O., SO, A. & DE SMEDT, T. 2008. Pharmacological inhibition of nicotinamide phosphoribosyltransferase/visfatin enzymatic activity identifies a new inflammatory pathway linked to NAD. *PLoS One,* 3**,** e2267.

CAMACHO-PEREIRA, J., TARRAGÓ, M. G., CHINI, C. C. S., NIN, V., ESCANDE, C., WARNER, G. M., PURANIK, A. S., SCHOON, R. A., REID, J. M., GALINA, A. & CHINI, E. N. 2016. CD38 Dictates Age-Related NAD Decline and Mitochondrial Dysfunction through an SIRT3-Dependent Mechanism. *Cell Metab,* 23**,** 1127-1139.

CAMERON, A. M., CASTOLDI, A., SANIN, D. E., FLACHSMANN, L. J., FIELD, C. S., PULESTON, D. J., KYLE, R. L., PATTERSON, A. E., HÄSSLER, F., BUESCHER, J. M., KELLY, B., PEARCE, E. L. & PEARCE, E. J. 2019. Inflammatory macrophage dependence on NAD+ salvage is a consequence of reactive oxygen species–mediated DNA damage. *Nature Immunology,* 20**,** 420-432.

CAO, X., WU, Y., HONG, H. & TIAN, X. Y. 2022. Sirtuin 3 Dependent and Independent Effects of NAD(+) to Suppress Vascular Inflammation and Improve Endothelial Function in Mice. *Antioxidants (Basel),* 11.

CARSON, J. A. S., LICHTENSTEIN, A. H., ANDERSON, C. A. M., APPEL, L. J., KRIS-ETHERTON, P. M., MEYER, K. A., PETERSEN, K., POLONSKY, T. & HORN, L. V. 2020. Dietary Cholesterol and Cardiovascular Risk: A Science Advisory From the American Heart Association. *Circulation,* 141**,** e39-e53.

CHANG, C. H., CURTIS, J. D., MAGGI, L. B., JR., FAUBERT, B., VILLARINO, A. V., O'SULLIVAN, D., HUANG, S. C., VAN DER WINDT, G. J., BLAGIH, J., QIU, J., WEBER, J. D., PEARCE, E. J., JONES, R. G. & PEARCE, E. L. 2013. Posttranscriptional control of T cell effector function by aerobic glycolysis. *Cell,* 153**,** 1239-51.

CHEN, Y., YANG, M., HUANG, W., CHEN, W., ZHAO, Y., SCHULTE, M. L., VOLBERDING, P., GERBEC, Z., ZIMMERMANN, M. T., ZEIGHAMI, A., DEMOS, W., ZHANG, J., KNAACK, D. A., SMITH, B. C., CUI, W., MALARKANNAN, S., SODHI, K., SHAPIRO, J. I., XIE, Z., SAHOO, D. & SILVERSTEIN, R. L. 2019. Mitochondrial Metabolic Reprogramming by CD36 Signaling Drives Macrophage Inflammatory Responses. *Circ Res,* 125**,** 1087-1102.

CHENG, S. C., QUINTIN, J., CRAMER, R. A., SHEPARDSON, K. M., SAEED, S., KUMAR, V., GIAMARELLOS-BOURBOULIS, E. J., MARTENS, J. H., RAO, N. A., AGHAJANIREFAH, A., MANJERI, G. R., LI, Y., IFRIM, D. C., ARTS, R. J., VAN DER VEER, B. M., DEEN, P. M., LOGIE, C., O'NEILL, L. A., WILLEMS, P., VAN DE VEERDONK, F. L., VAN DER MEER, J. W., NG, A., JOOSTEN, L. A., WIJMENGA, C., STUNNENBERG, H. G., XAVIER, R. J. & NETEA, M. G. 2014. mTOR- and HIF-1α-mediated aerobic glycolysis as metabolic basis for trained immunity. *Science,* 345**,** 1250684.

CHRIST, A., GÜNTHER, P., LAUTERBACH, M. A. R., DUEWELL, P., BISWAS, D., PELKA, K., SCHOLZ, C. J., OOSTING, M., HAENDLER, K., BASSLE, K., KLEE, K., SCHULTE-SCHREPPING, J., ULAS, T., MOORLAG, S., KUMAR, V., PARK, M. H., JOOSTEN, L. A. B., GROH, L. A., RIKSEN, N. P., ESPEVIK, T., SCHLITZER, A., LI, Y., FITZGERALD, M. L., NETEA, M. G., SCHULTZE, J. L. & LATZ, E. 2018. Western Diet Triggers NLRP3-Dependent Innate Immune Reprogramming. *Cell,* 172**,** 162-175.e14.

CLARKE, M. C. H., FIGG, N., MAGUIRE, J. J., DAVENPORT, A. P., GODDARD, M., LITTLEWOOD, T. D. & BENNETT, M. R. 2006. Apoptosis of vascular smooth muscle cells induces features of plaque vulnerability in atherosclerosis. *Nature Medicine,* 12**,** 1075-1080.

COLLINS, P. B. & CHAYKIN, S. 1972. The management of nicotinamide and nicotinic acid in the mouse. *J Biol Chem,* 247**,** 778-83.

COLOMBO, G., TRAVELLI, C., PORTA, C. & GENAZZANI, A. A. 2022. Extracellular nicotinamide phosphoribosyltransferase boosts IFNγ-induced macrophage polarization independently of TLR4. *iScience,* 25**,** 104147.

CORNIER, M. A., DABELEA, D., HERNANDEZ, T. L., LINDSTROM, R. C., STEIG, A. J., STOB, N. R., VAN PELT, R. E., WANG, H. & ECKEL, R. H. 2008. The metabolic syndrome. *Endocr Rev,* 29**,** 777-822.

COVARRUBIAS, A. J., AKSOYLAR, H. I., YU, J., SNYDER, N. W., WORTH, A. J., IYER, S. S., WANG, J., BEN-SAHRA, I., BYLES, V., POLYNNE-STAPORNKUL, T., ESPINOSA, E. C., LAMMING, D., MANNING, B. D., ZHANG, Y., BLAIR, I. A. & HORNG, T. 2016. Akt-mTORC1 signaling

regulates Acly to integrate metabolic input to control of macrophage activation. *Elife,* 5.

COVARRUBIAS, A. J., KALE, A., PERRONE, R., LOPEZ-DOMINGUEZ, J. A., PISCO, A. O., KASLER, H. G., SCHMIDT, M. S., HECKENBACH, I., KWOK, R., WILEY, C. D., WONG, H. S., GIBBS, E., IYER, S. S., BASISTY, N., WU, Q., KIM, I. J., SILVA, E., VITANGCOL, K., SHIN, K. O., LEE, Y. M., RILEY, R., BEN-SAHRA, I., OTT, M., SCHILLING, B., SCHEIBYE-KNUDSEN, M., ISHIHARA, K., QUAKE, S. R., NEWMAN, J., BRENNER, C., CAMPISI, J. & VERDIN, E. 2020. Senescent cells promote tissue NAD(+) decline during ageing via the activation of CD38(+) macrophages. *Nat Metab,* 2**,** 1265-1283.

DE KREUTZENBERG, S. V., CEOLOTTO, G., PAPPARELLA, I., BORTOLUZZI, A., SEMPLICINI, A., DALLA MAN, C., COBELLI, C., FADINI, G. P. & AVOGARO, A. 2010. Downregulation of the longevity-associated protein sirtuin 1 in insulin resistance and metabolic syndrome: potential biochemical mechanisms. *Diabetes,* 59**,** 1006-15.

DE PICCIOTTO, N. E., GANO, L. B., JOHNSON, L. C., MARTENS, C. R., SINDLER, A. L., MILLS, K. F., IMAI, S.-I. & SEALS, D. R. 2016. Nicotinamide mononucleotide supplementation reverses vascular dysfunction and oxidative stress with aging in mice. *Aging Cell,* 15**,** 522-530.

DE ROSA, V., GALGANI, M., PORCELLINI, A., COLAMATTEO, A., SANTOPAOLO, M., ZUCHEGNA, C., ROMANO, A., DE SIMONE, S., PROCACCINI, C., LA ROCCA, C., CARRIERI, P. B., MANISCALCO, G. T., SALVETTI, M., BUSCARINU, M. C., FRANZESE, A., MOZZILLO, E., LA CAVA, A. & MATARESE, G. 2015. Glycolysis controls the induction of human regulatory T cells by modulating the expression of FOXP3 exon 2 splicing variants. *Nat Immunol,* 16**,** 1174-84.

DIGBY, J. E., RUPARELIA, N. & CHOUDHURY, R. P. 2012. Niacin in Cardiovascular Disease: Recent Preclinical and Clinical Developments. *Arteriosclerosis, Thrombosis, and Vascular Biology,* 32**,** 582-588.

DIKALOVA, A. E., ITANI, H. A., NAZAREWICZ, R. R., MCMASTER, W. G., FLYNN, C. R., UZHACHENKO, R., FESSEL, J. P., GAMBOA, J. L., HARRISON, D. G. & DIKALOV, S. I. 2017. Sirt3 Impairment and SOD2 Hyperacetylation in Vascular Oxidative Stress and Hypertension. *Circ Res,* 121**,** 564-574.

DING, Y., GONG, W., ZHANG, S., SHEN, J., LIU, X., WANG, Y., CHEN, Y. & MENG, G. 2021. Protective role of sirtuin3 against oxidative stress and NLRP3 inflammasome in cholesterol accumulation and foam cell formation of macrophages with ox-LDL-stimulation. *Biochemical Pharmacology,* 192**,** 114665.

DUEWELL, P., KONO, H., RAYNER, K. J., SIROIS, C. M., VLADIMER, G., BAUERNFEIND, F. G., ABELA, G. S., FRANCHI, L., NUÑEZ, G., SCHNURR, M., ESPEVIK, T., LIEN, E., FITZGERALD, K. A., ROCK, K. L., MOORE, K. J., WRIGHT, S. D., HORNUNG, V. & LATZ, E. 2010. NLRP3 inflammasomes are required for atherogenesis and activated by cholesterol crystals. *Nature,* 464**,** 1357-61.

ELKHAL, A., RODRIGUEZ CETINA BIEFER, H., HEINBOKEL, T., UEHARA, H., QUANTE, M., SEYDA, M., SCHUITENMAKER, J. M., KRENZIEN, F., CAMACHO, V., DE LA FUENTE, M. A., GHIRAN, I. & TULLIUS, S. G. 2016. NAD(+) regulates Treg cell fate and promotes allograft survival via a systemic IL-10 production that is CD4(+) CD25(+) Foxp3(+) T cells independent. *Sci Rep,* 6**,** 22325.

FELICI, R., LAPUCCI, A., RAMAZZOTTI, M. & CHIARUGI, A. 2013. Insight into molecular and functional properties of NMNAT3 reveals new hints of NAD homeostasis within human mitochondria. *PLoS One,* 8**,** e76938.

FENG, S., BOWDEN, N., FRAGIADAKI, M., SOUILHOL, C., HSIAO, S., MAHMOUD, M., ALLEN, S., PIRRI, D., AYLLON, B. T., AKHTAR, S., THOMPSON, A. A. R., JO, H., WEBER, C., RIDGER, V., SCHOBER, A. & EVANS, P. C. 2017. Mechanical Activation of Hypoxia-Inducible Factor 1α Drives Endothelial Dysfunction at Atheroprone Sites. *Arterioscler Thromb Vasc Biol,* 37**,** 2087-2101.

FERNANDEZ, D. M. & GIANNARELLI, C. 2022. Immune cell profiling in atherosclerosis: role in research and precision medicine. *Nature Reviews Cardiology,* 19**,** 43-58.

FINLEY, L. W., HAAS, W., DESQUIRET-DUMAS, V., WALLACE, D. C., PROCACCIO, V., GYGI, S. P. & HAIGIS, M. C. 2011. Succinate dehydrogenase is a direct target of sirtuin 3 deacetylase activity. *PLoS One,* 6**,** e23295.

FÖRSTERMANN, U., XIA, N. & LI, H. 2017. Roles of Vascular Oxidative Stress and Nitric Oxide in the Pathogenesis of Atherosclerosis. *Circulation Research,* 120**,** 713-735.

FORTUNATO, C., MAZZOLA, F. & RAFFAELLI, N. 2022. The key role of the NAD biosynthetic enzyme nicotinamide mononucleotide adenylyltransferase in regulating cell functions. *IUBMB Life,* 74**,** 562-572.

FRACASSI, F., CREA, F., SUGIYAMA, T., YAMAMOTO, E., UEMURA, S., VERGALLO, R., PORTO, I., LEE, H., FUJIMOTO, J., FUSTER, V. & JANG, I.-K. 2019. Healed Culprit Plaques in Patients With Acute Coronary Syndromes. *Journal of the American College of Cardiology,* 73**,** 2253-2263.

FRANCK, G., EVEN, G., GAUTIER, A., SALINAS, M., LOSTE, A., PROCOPIO, E., GASTON, A.-T., MORVAN, M., DUPONT, S., DESCHILDRE, C., BERISSI, S., LASCHET, J., NATAF, P., NICOLETTI, A., MICHEL, J.-B. & CALIGIURI, G. 2018. Haemodynamic stress-induced breaches of the arterial intima trigger inflammation and drive atherogenesis. *European Heart Journal,* 40**,** 928-937.

GETZ, G. S. & REARDON, C. A. 2009. Apoprotein E as a lipid transport and signaling protein in the blood, liver, and artery wall. *J Lipid Res,* 50 Suppl**,** S156-61.

GONG, H., LIU, J., XUE, Z., WANG, W., LI, C., XU, F., DU, Y. & LYU, X. 2022. SIRT3 attenuates coronary atherosclerosis in diabetic patients by regulating endothelial cell function. *J Clin Lab Anal,* 36**,** e24586.

GORENNE, I., KUMAR, S., GRAY, K., FIGG, N., YU, H., MERCER, J. & BENNETT, M. 2013. Vascular smooth muscle cell sirtuin 1 protects against DNA damage and inhibits atherosclerosis. *Circulation,* 127**,** 386-96.

GROOTAERT, M. O. J. & BENNETT, M. R. 2022. Sirtuins in atherosclerosis: guardians of healthspan and therapeutic targets. *Nature Reviews Cardiology,* 19**,** 668-683.

GROOTAERT, M. O. J., FINIGAN, A., FIGG, N. L., URYGA, A. K. & BENNETT, M. R. 2021. SIRT6 Protects Smooth Muscle Cells From Senescence and Reduces Atherosclerosis. *Circ Res,* 128**,** 474-491.

HALVORSEN, B., ESPELAND, M. Z., ANDERSEN, G., YNDESTAD, A., SAGEN, E. L., RASHIDI, A., KNUDSEN, E. C., SKJELLAND, M., SKAGEN, K. R., KROHG-SØRENSEN, K., HOLM, S., RITSCHEL, V., HOLVEN, K. B.,

BIESSEN, E. A., AUKRUST, P. & DAHL, T. B. 2015. Increased expression of NAMPT in PBMC from patients with acute coronary syndrome and in inflammatory M1 macrophages. *Atherosclerosis,* 243**,** 204-10.

HARTWIG, H., SILVESTRE-ROIG, C., HENDRIKSE, J., BECKERS, L., PAULIN, N., VAN DER HEIDEN, K., BRASTER, Q., DRECHSLER, M., DAEMEN, M. J., LUTGENS, E. & SOEHNLEIN, O. 2015. Atherosclerotic Plaque Destabilization in Mice: A Comparative Study. *PLoS One,* 10**,** e0141019.

HASCHEMI, A., KOSMA, P., GILLE, L., EVANS, C. R., BURANT, C. F., STARKL, P., KNAPP, B., HAAS, R., SCHMID, J. A., JANDL, C., AMIR, S., LUBEC, G., PARK, J., ESTERBAUER, H., BILBAN, M., BRIZUELA, L., POSPISILIK, J. A., OTTERBEIN, L. E. & WAGNER, O. 2012. The sedoheptulose kinase CARKL directs macrophage polarization through control of glucose metabolism. *Cell Metab,* 15**,** 813-26.

HE, J., ZHANG, G., PANG, Q., YU, C., XIONG, J., ZHU, J. & CHEN, F. 2017. SIRT6 reduces macrophage foam cell formation by inducing autophagy and cholesterol efflux under ox-LDL condition. *Febs j,* 284**,** 1324-1337.

HERRINGTON, W., LACEY, B., SHERLIKER, P., ARMITAGE, J. & LEWINGTON, S. 2016. Epidemiology of Atherosclerosis and the Potential to Reduce the Global Burden of Atherothrombotic Disease. *Circulation Research,* 118**,** 535-546.

HIRSCHEY, M. D., SHIMAZU, T., GOETZMAN, E., JING, E., SCHWER, B., LOMBARD, D. B., GRUETER, C. A., HARRIS, C., BIDDINGER, S., ILKAYEVA, O. R., STEVENS, R. D., LI, Y., SAHA, A. K., RUDERMAN, N. B., BAIN, J. R., NEWGARD, C. B., FARESE, R. V., JR., ALT, F. W., KAHN, C. R. & VERDIN, E. 2010. SIRT3 regulates mitochondrial fatty-acid oxidation by reversible enzyme deacetylation. *Nature,* 464**,** 121-5.

HOUTKOOPER, R. H., CANTÓ, C., WANDERS, R. J. & AUWERX, J. 2010. The secret life of NAD+: an old metabolite controlling new metabolic signaling pathways. *Endocr Rev,* 31**,** 194-223.

IGARASHI, M., NAKAGAWA-NAGAHAMA, Y., MIURA, M., KASHIWABARA, K., YAKU, K., SAWADA, M., SEKINE, R., FUKAMIZU, Y., SATO, T., SAKURAI, T., SATO, J., INO, K., KUBOTA, N., NAKAGAWA, T., KADOWAKI, T. & YAMAUCHI, T. 2022. Chronic nicotinamide mononucleotide supplementation elevates blood nicotinamide adenine dinucleotide levels and alters muscle function in healthy older men. *NPJ Aging,* 8**,** 5.

IJICHI, H., ICHIYAMA, A. & HAYAISHI, O. 1966. Studies on the biosynthesis of nicotinamide adenine dinucleotide. 3. Comparative in vivo studies on nicotinic acid, nicotinamide, and quinolinic acid as precursors of nicotinamide adenine dinucleotide. *J Biol Chem,* 241**,** 3701-7.

IMAI, S.-I., ARMSTRONG, C. M., KAEBERLEIN, M. & GUARENTE, L. 2000. Transcriptional silencing and longevity protein Sir2 is an NAD-dependent histone deacetylase. *Nature,* 403**,** 795-800.

IMI, Y., AMANO, R., KASAHARA, N., OBANA, Y. & HOSOOKA, T. 2023. Nicotinamide mononucleotide induces lipolysis by regulating ATGL expression via the SIRT1-AMPK axis in adipocytes. *Biochemistry and Biophysics Reports,* 34**,** 101476.

IP, W. K. E., HOSHI, N., SHOUVAL, D. S., SNAPPER, S. & MEDZHITOV, R. 2017. Anti-inflammatory effect of IL-10 mediated by metabolic reprogramming of macrophages. *Science,* 356**,** 513-519.

ISHIBASHI, S., GOLDSTEIN, J. L., BROWN, M. S., HERZ, J. & BURNS, D. K. 1994a. Massive xanthomatosis and atherosclerosis in cholesterol-fed low density lipoprotein receptor-negative mice. *The Journal of Clinical Investigation,* 93**,** 1885-1893.

ISHIBASHI, S., HERZ, J., MAEDA, N., GOLDSTEIN, J. L. & BROWN, M. S. 1994b. The two-receptor model of lipoprotein clearance: tests of the hypothesis in "knockout" mice lacking the low density lipoprotein receptor, apolipoprotein E, or both proteins. *Proceedings of the National Academy of Sciences,* 91**,** 4431-4435.

JAFARI-AZAD, A., HOSSEINI, L., RAJABI, M., HØILUND-CARLSEN, P. F., VAFAEE, M. S., FEYZIZADEH, S. & BADALZADEH, R. 2021. Nicotinamide mononucleotide and melatonin counteract myocardial ischemia-reperfusion injury by activating SIRT3/FOXO1 and reducing apoptosis in aged male rats. *Molecular Biology Reports,* 48**,** 3089-3096.

JHA, ABHISHEK K., HUANG, STANLEY C.-C., SERGUSHICHEV, A., LAMPROPOULOU, V., IVANOVA, Y., LOGINICHEVA, E., CHMIELEWSKI, K., STEWART, KELLY M., ASHALL, J., EVERTS, B., PEARCE, EDWARD J., DRIGGERS, EDWARD M. & ARTYOMOV, MAXIM N. 2015. Network Integration of Parallel Metabolic and Transcriptional Data Reveals Metabolic Modules that Regulate Macrophage Polarization. *Immunity,* 42**,** 419-430.

KE, Y., WANG, C., ZHANG, J., ZHONG, X., WANG, R., ZENG, X. & BA, X. 2019. The Role of PARPs in Inflammation-and Metabolic-Related Diseases: Molecular Mechanisms and Beyond. *Cells,* 8.

KIMURA, S., ICHIKAWA, M., SUGAWARA, S., KATAGIRI, T., HIRASAWA, Y., ISHIKAWA, T., MATSUNAGA, W. & GOTOH, A. 2022. Nicotinamide Mononucleotide Is Safely Metabolized and Significantly Reduces Blood Triglyceride Levels in Healthy Individuals. *Cureus,* 14**,** e28812.

KOLTSOVA, E. K., GARCIA, Z., CHODACZEK, G., LANDAU, M., MCARDLE, S., SCOTT, S. R., VON VIETINGHOFF, S., GALKINA, E., MILLER, Y. I., ACTON, S. T. & LEY, K. 2012. Dynamic T cell-APC interactions sustain chronic inflammation in atherosclerosis. *J Clin Invest,* 122**,** 3114-26.

KUANG, H., YANG, F., ZHANG, Y., WANG, T. & CHEN, G. 2018. The Impact of Egg Nutrient Composition and Its Consumption on Cholesterol Homeostasis. *Cholesterol,* 2018**,** 6303810.

KUHNAST, S., LOUWE, M. C., HEEMSKERK, M. M., PIETERMAN, E. J., VAN KLINKEN, J. B., VAN DEN BERG, S. A., SMIT, J. W., HAVEKES, L. M., RENSEN, P. C., VAN DER HOORN, J. W., PRINCEN, H. M. & JUKEMA, J. W. 2013. Niacin Reduces Atherosclerosis Development in APOE*3Leiden.CETP Mice Mainly by Reducing NonHDL-Cholesterol. *PLoS One,* 8**,** e66467.

LEITINGER, N., TYNER, T. R., OSLUND, L., RIZZA, C., SUBBANAGOUNDER, G., LEE, H., SHIH, P. T., MACKMAN, N., TIGYI, G., TERRITO, M. C., BERLINER, J. A. & VORA, D. K. 1999. Structurally similar oxidized phospholipids differentially regulate endothelial binding of monocytes and neutrophils. *Proc Natl Acad Sci U S A,* 96**,** 12010-5.

LEWIS, E. A., MUÑIZ-ANQUELA, R., REDONDO-ANGULO, I., GONZÁLEZ-CINTADO, L., LABRADOR-CANTARERO, V. & BENTZON, J. F. 2023. Capacity for LDL (Low-Density Lipoprotein) Retention Predicts the Course of

Atherogenesis in the Murine Aortic Arch. *Arterioscler Thromb Vasc Biol,* 43**,** 637-649.
LI, Y., ZHANG, Y., DORWEILER, B., CUI, D., WANG, T., WOO, C. W., BRUNKAN, C. S., WOLBERGER, C., IMAI, S. & TABAS, I. 2008. Extracellular Nampt promotes macrophage survival via a nonenzymatic interleukin-6/STAT3 signaling mechanism. *J Biol Chem,* 283**,** 34833-43.
LIBBY, P. 2021. The changing landscape of atherosclerosis. *Nature,* 592**,** 524-533.
LICHTMAN, A. H., CLINTON, S. K., IIYAMA, K., CONNELLY, P. W., LIBBY, P. & CYBULSKY, M. I. 1999. Hyperlipidemia and Atherosclerotic Lesion Development in LDL Receptor–Deficient Mice Fed Defined Semipurified Diets With and Without Cholate. *Arteriosclerosis, Thrombosis, and Vascular Biology,* 19**,** 1938-1944.
LIU, L., SU, X., QUINN, W. J., 3RD, HUI, S., KRUKENBERG, K., FREDERICK, D. W., REDPATH, P., ZHAN, L., CHELLAPPA, K., WHITE, E., MIGAUD, M., MITCHISON, T. J., BAUR, J. A. & RABINOWITZ, J. D. 2018a. Quantitative Analysis of NAD Synthesis-Breakdown Fluxes. *Cell Metab,* 27**,** 1067-1080.e5.
LIU, P., HUANG, G., WEI, T., GAO, J., HUANG, C., SUN, M., ZHU, L. & SHEN, W. 2018b. Sirtuin 3-induced macrophage autophagy in regulating NLRP3 inflammasome activation. *Biochimica et Biophysica Acta (BBA) - Molecular Basis of Disease,* 1864**,** 764-777.
LU, J., WANG, M., CHEN, Y., SONG, H., WEN, D., TU, J., GUO, Y. & LIU, Z. 2023. NAMPT inhibition reduces macrophage inflammation through the NAD+/PARP1 pathway to attenuate liver ischemia–reperfusion injury. *Chemico-Biological Interactions,* 369**,** 110294.
LUKASOVA, M., MALAVAL, C., GILLE, A., KERO, J. & OFFERMANNS, S. 2011. Nicotinic acid inhibits progression of atherosclerosis in mice through its receptor GPR109A expressed by immune cells. *J Clin Invest,* 121**,** 1163-73.
MAN, J. J., BECKMAN, J. A. & JAFFE, I. Z. 2020. Sex as a Biological Variable in Atherosclerosis. *Circulation Research,* 126**,** 1297-1319.
MANSUKHANI, N. A., WANG, Z., SHIVELY, V. P., KELLY, M. E., VERCAMMEN, J. M. & KIBBE, M. R. 2017. Sex Differences in the LDL Receptor Knockout Mouse Model of Atherosclerosis. *Artery Res,* 20**,** 8-11.
MARTINON, F., BURNS, K. & TSCHOPP, J. 2002. The inflammasome: a molecular platform triggering activation of inflammatory caspases and processing of proIL-beta. *Mol Cell,* 10**,** 417-26.
MASSUDI, H., GRANT, R., BRAIDY, N., GUEST, J., FARNSWORTH, B. & GUILLEMIN, G. J. 2012. Age-associated changes in oxidative stress and NAD+ metabolism in human tissue. *PLoS One,* 7**,** e42357.
MCREYNOLDS, M. R., CHELLAPPA, K. & BAUR, J. A. 2020. Age-related NAD(+) decline. *Exp Gerontol,* 134**,** 110888.
MENDEZ-LARA, K. A., LETELIER, N., FARRE, N., DIARTE-ANAZCO, E. M. G., NIETO-NICOLAU, N., RODRIGUEZ-MILLAN, E., SANTOS, D., PALLARES, V., ESCOLA-GIL, J. C., VAZQUEZ DEL OLMO, T., LERMA, E., CAMACHO, M., CASAROLI-MARANO, R. P., VALLEDOR, A. F., BLANCO-VACA, F. & JULVE, J. 2020. Nicotinamide Prevents Apolipoprotein B-Containing Lipoprotein Oxidation, Inflammation and Atherosclerosis in Apolipoprotein E-Deficient Mice. *Antioxidants (Basel),* 9.
MENG, F., QIAN, M., PENG, B., PENG, L., WANG, X., ZHENG, K., LIU, Z., TANG, X., ZHANG, S., SUN, S., CAO, X., PANG, Q., ZHAO, B., MA, W.,

SONGYANG, Z., XU, B., ZHU, W. G., XU, X. & LIU, B. 2020. Synergy between SIRT1 and SIRT6 helps recognize DNA breaks and potentiates the DNA damage response and repair in humans and mice. *Elife,* 9.

MENU, P., PELLEGRIN, M., AUBERT, J. F., BOUZOURENE, K., TARDIVEL, A., MAZZOLAI, L. & TSCHOPP, J. 2011. Atherosclerosis in ApoE-deficient mice progresses independently of the NLRP3 inflammasome. *Cell Death Dis,* 2**,** e137.

MERAT, S., CASANADA, F., SUTPHIN, M., PALINSKI, W. & REAVEN, P. D. 1999. Western-Type Diets Induce Insulin Resistance and Hyperinsulinemia in LDL Receptor-Deficient Mice But Do Not Increase Aortic Atherosclerosis Compared With Normoinsulinemic Mice in Which Similar Plasma Cholesterol Levels Are Achieved by a Fructose-Rich Diet. *Arteriosclerosis, Thrombosis, and Vascular Biology,* 19**,** 1223-1230.

MICHALEK, R. D., GERRIETS, V. A., JACOBS, S. R., MACINTYRE, A. N., MACIVER, N. J., MASON, E. F., SULLIVAN, S. A., NICHOLS, A. G. & RATHMELL, J. C. 2011. Cutting edge: distinct glycolytic and lipid oxidative metabolic programs are essential for effector and regulatory CD4+ T cell subsets. *J Immunol,* 186**,** 3299-303.

MILLER, Y. I., CHOI, S. H., WIESNER, P., FANG, L., HARKEWICZ, R., HARTVIGSEN, K., BOULLIER, A., GONEN, A., DIEHL, C. J., QUE, X., MONTANO, E., SHAW, P. X., TSIMIKAS, S., BINDER, C. J. & WITZTUM, J. L. 2011. Oxidation-specific epitopes are danger-associated molecular patterns recognized by pattern recognition receptors of innate immunity. *Circ Res,* 108**,** 235-48.

MILLS, K. F., YOSHIDA, S., STEIN, L. R., GROZIO, A., KUBOTA, S., SASAKI, Y., REDPATH, P., MIGAUD, M. E., APTE, R. S., UCHIDA, K., YOSHINO, J. & IMAI, S. I. 2016. Long-Term Administration of Nicotinamide Mononucleotide Mitigates Age-Associated Physiological Decline in Mice. *Cell Metab,* 24**,** 795-806.

MINHAS, P. S., LIU, L., MOON, P. K., JOSHI, A. U., DOVE, C., MHATRE, S., CONTREPOIS, K., WANG, Q., LEE, B. A., CORONADO, M., BERNSTEIN, D., SNYDER, M. P., MIGAUD, M., MAJETI, R., MOCHLY-ROSEN, D., RABINOWITZ, J. D. & ANDREASSON, K. I. 2019. Macrophage de novo NAD+ synthesis specifies immune function in aging and inflammation. *Nature Immunology,* 20**,** 50-63.

MOORE, K. J. & FREEMAN, M. W. 2006. Scavenger Receptors in Atherosclerosis. *Arteriosclerosis, Thrombosis, and Vascular Biology,* 26**,** 1702-1711.

NIDORF, S. M., EIKELBOOM, J. W., BUDGEON, C. A. & THOMPSON, P. L. 2013. Low-dose colchicine for secondary prevention of cardiovascular disease. *J Am Coll Cardiol,* 61**,** 404-410.

NIKIFOROV, A., DÖLLE, C., NIERE, M. & ZIEGLER, M. 2011. Pathways and subcellular compartmentation of NAD biosynthesis in human cells: from entry of extracellular precursors to mitochondrial NAD generation. *J Biol Chem,* 286**,** 21767-78.

PATELLA, F., SCHUG, Z. T., PERSI, E., NEILSON, L. J., ERAMI, Z., AVANZATO, D., MAIONE, F., HERNANDEZ-FERNAUD, J. R., MACKAY, G., ZHENG, L., REID, S., FREZZA, C., GIRAUDO, E., FIORIO PLA, A., ANDERSON, K., RUPPIN, E., GOTTLIEB, E. & ZANIVAN, S. 2015. Proteomics-based metabolic modeling reveals that fatty acid oxidation (FAO) controls endothelial cell (EC) permeability. *Mol Cell Proteomics,* 14**,** 621-34.

PLUMP, A. S., SMITH, J. D., HAYEK, T., AALTO-SETÄLÄ, K., WALSH, A., VERSTUYFT, J. G., RUBIN, E. M. & BRESLOW, J. L. 1992. Severe hypercholesterolemia and atherosclerosis in apolipoprotein E-deficient mice created by homologous recombination in ES cells. *Cell,* 71**,** 343-53.

POLYZOS, K. A., OVCHINNIKOVA, O., BERG, M., BAUMGARTNER, R., AGARDH, H., PIRAULT, J., GISTERÅ, A., ASSINGER, A., LAGUNA-FERNANDEZ, A., BÄCK, M., HANSSON, G. K. & KETELHUTH, D. F. 2015. Inhibition of indoleamine 2,3-dioxygenase promotes vascular inflammation and increases atherosclerosis in Apoe-/- mice. *Cardiovasc Res,* 106**,** 295-302.

PREISS, J. & HANDLER, P. 1957. Enzymatic synthesis of nicotinamide mononucleotide. *J Biol Chem,* 225**,** 759-70.

PUYLAERT, P., ZUREK, M., RAYNER, K. J., MEYER, G. R. Y. D. & MARTINET, W. 2022. Regulated Necrosis in Atherosclerosis. *Arteriosclerosis, Thrombosis, and Vascular Biology,* 42**,** 1283-1306.

QIU, Y., XU, S., CHEN, X., WU, X., ZHOU, Z., ZHANG, J., TU, Q., DONG, B., LIU, Z., HE, J., ZHANG, X., LIU, S., SU, C., HUANG, H., XIA, W. & TAO, J. 2023. NAD(+) exhaustion by CD38 upregulation contributes to blood pressure elevation and vascular damage in hypertension. *Signal Transduct Target Ther,* 8**,** 353.

QUE, X., HUNG, M. Y., YEANG, C., GONEN, A., PROHASKA, T. A., SUN, X., DIEHL, C., MÄÄTTÄ, A., GADDIS, D. E., BOWDEN, K., PATTISON, J., MACDONALD, J. G., YLÄ-HERTTUALA, S., MELLON, P. L., HEDRICK, C. C., LEY, K., MILLER, Y. I., GLASS, C. K., PETERSON, K. L., BINDER, C. J., TSIMIKAS, S. & WITZTUM, J. L. 2018. Oxidized phospholipids are proinflammatory and proatherogenic in hypercholesterolaemic mice. *Nature,* 558**,** 301-306.

RAHAMAN, S. O., LENNON, D. J., FEBBRAIO, M., PODREZ, E. A., HAZEN, S. L. & SILVERSTEIN, R. L. 2006. A CD36-dependent signaling cascade is necessary for macrophage foam cell formation. *Cell Metab,* 4**,** 211-21.

RAJAMÄKI, K., LAPPALAINEN, J., OÖRNI, K., VÄLIMÄKI, E., MATIKAINEN, S., KOVANEN, P. T. & EKLUND, K. K. 2010. Cholesterol crystals activate the NLRP3 inflammasome in human macrophages: a novel link between cholesterol metabolism and inflammation. *PLoS One,* 5**,** e11765.

RENARD, C. B., KRAMER, F., JOHANSSON, F., LAMHARZI, N., TANNOCK, L. R., VON HERRATH, M. G., CHAIT, A. & BORNFELDT, K. E. 2004. Diabetes and diabetes-associated lipid abnormalities have distinct effects on initiation and progression of atherosclerotic lesions. *J Clin Invest,* 114**,** 659-68.

RIDKER, P. M., EVERETT, B. M., THUREN, T., MACFADYEN, J. G., CHANG, W. H., BALLANTYNE, C., FONSECA, F., NICOLAU, J., KOENIG, W., ANKER, S. D., KASTELEIN, J. J. P., CORNEL, J. H., PAIS, P., PELLA, D., GENEST, J., CIFKOVA, R., LORENZATTI, A., FORSTER, T., KOBALAVA, Z., VIDA-SIMITI, L., FLATHER, M., SHIMOKAWA, H., OGAWA, H., DELLBORG, M., ROSSI, P. R. F., TROQUAY, R. P. T., LIBBY, P. & GLYNN, R. J. 2017. Antiinflammatory Therapy with Canakinumab for Atherosclerotic Disease. *New England Journal of Medicine,* 377**,** 1119-1131.

RIUS, J., GUMA, M., SCHACHTRUP, C., AKASSOGLOU, K., ZINKERNAGEL, A. S., NIZET, V., JOHNSON, R. S., HADDAD, G. G. & KARIN, M. 2008. NF-kappaB links innate immunity to the hypoxic response through transcriptional regulation of HIF-1alpha. *Nature,* 453**,** 807-11.

ROCHE-MOLINA, M., SANZ-ROSA, D., CRUZ, F. M., GARCÍA-PRIETO, J., LÓPEZ, S., ABIA, R., MURIANA, F. J., FUSTER, V., IBÁÑEZ, B. & BERNAL, J. A. 2015. Induction of sustained hypercholesterolemia by single adeno-associated virus-mediated gene transfer of mutant hPCSK9. *Arterioscler Thromb Vasc Biol,* 35**,** 50-9.

ROICHMAN, A., ELHANATI, S., AON, M. A., ABRAMOVICH, I., DI FRANCESCO, A., SHAHAR, Y., AVIVI, M. Y., SHURGI, M., RUBINSTEIN, A., WIESNER, Y., SHUCHAMI, A., PETROVER, Z., LEBENTHAL-LOINGER, I., YARON, O., LYASHKOV, A., UBAIDA-MOHIEN, C., KANFI, Y., LERRER, B., FERNÁNDEZ-MARCOS, P. J., SERRANO, M., GOTTLIEB, E., DE CABO, R. & COHEN, H. Y. 2021. Restoration of energy homeostasis by SIRT6 extends healthy lifespan. *Nat Commun,* 12**,** 3208.

ROTHWELL, P. M., COULL, A. J., SILVER, L. E., FAIRHEAD, J. F., GILES, M. F., LOVELOCK, C. E., REDGRAVE, J. N., BULL, L. M., WELCH, S. J., CUTHBERTSON, F. C., BINNEY, L. E., GUTNIKOV, S. A., ANSLOW, P., BANNING, A. P., MANT, D. & MEHTA, Z. 2005. Population-based study of event-rate, incidence, case fatality, and mortality for all acute vascular events in all arterial territories (Oxford Vascular Study). *Lancet,* 366**,** 1773-83.

SCHREYER, S. A., VICK, C., LYSTIG, T. C., MYSTKOWSKI, P. & LEBOEUF, R. C. 2002. LDL receptor but not apolipoprotein E deficiency increases diet-induced obesity and diabetes in mice. *Am J Physiol Endocrinol Metab,* 282**,** E207-14.

SCHWARZMANN, L., PLIQUETT, R. U., SIMM, A. & BARTLING, B. 2021. Sex-related differences in human plasma NAD+/NADH levels depend on age. *Biosci Rep,* 41.

SHEEDY, F. J., GREBE, A., RAYNER, K. J., KALANTARI, P., RAMKHELAWON, B., CARPENTER, S. B., BECKER, C. E., EDIRIWEERA, H. N., MULLICK, A. E., GOLENBOCK, D. T., STUART, L. M., LATZ, E., FITZGERALD, K. A. & MOORE, K. J. 2013. CD36 coordinates NLRP3 inflammasome activation by facilitating intracellular nucleation of soluble ligands into particulate ligands in sterile inflammation. *Nat Immunol,* 14**,** 812-20.

SHI, L. Z., WANG, R., HUANG, G., VOGEL, P., NEALE, G., GREEN, D. R. & CHI, H. 2011. HIF1alpha-dependent glycolytic pathway orchestrates a metabolic checkpoint for the differentiation of TH17 and Treg cells. *J Exp Med,* 208**,** 1367-76.

SHIM, D.-W., CHO, H.-J., HWANG, I., JUNG, T.-Y., KIM, H.-S., RYU, J. H. & YU, J.-W. 2021. Intracellular NAD+ Depletion Confers a Priming Signal for NLRP3 Inflammasome Activation. *Frontiers in Immunology,* 12.

SHIMAZU, T., HIRSCHEY, M. D., HUA, L., DITTENHAFER-REED, K. E., SCHWER, B., LOMBARD, D. B., LI, Y., BUNKENBORG, J., ALT, F. W., DENU, J. M., JACOBSON, M. P. & VERDIN, E. 2010. SIRT3 deacetylates mitochondrial 3-hydroxy-3-methylglutaryl CoA synthase 2 and regulates ketone body production. *Cell Metab,* 12**,** 654-61.

SICA, A. & MANTOVANI, A. 2012. Macrophage plasticity and polarization: in vivo veritas. *J Clin Invest,* 122**,** 787-95.

SOCIALI, G., GROZIO, A., CAFFA, I., SCHUSTER, S., BECHERINI, P., DAMONTE, P., STURLA, L., FRESIA, C., PASSALACQUA, M., MAZZOLA, F., RAFFAELLI, N., GARTEN, A., KIESS, W., CEA, M., NENCIONI, A. & BRUZZONE, S. 2019. SIRT6 deacetylase activity regulates NAMPT activity and NAD(P)(H) pools in cancer cells. *Faseb j,* 33**,** 3704-3717.

STEMME, S., FABER, B., HOLM, J., WIKLUND, O., WITZTUM, J. L. & HANSSON, G. K. 1995. T lymphocytes from human atherosclerotic plaques recognize oxidized low density lipoprotein. *Proc Natl Acad Sci U S A,* 92**,** 3893-7.

SUNDARESAN, N. R., GUPTA, M., KIM, G., RAJAMOHAN, S. B., ISBATAN, A. & GUPTA, M. P. 2009. Sirt3 blocks the cardiac hypertrophic response by augmenting Foxo3a-dependent antioxidant defense mechanisms in mice. *J Clin Invest,* 119**,** 2758-71.

SURWIT, R. S., KUHN, C. M., COCHRANE, C., MCCUBBIN, J. A. & FEINGLOS, M. N. 1988. Diet-Induced Type II Diabetes in C57BL/6J Mice. *Diabetes,* 37**,** 1163-1167.

TABAS, I., WILLIAMS, K. J. & BORÉN, J. 2007. Subendothelial lipoprotein retention as the initiating process in atherosclerosis: update and therapeutic implications. *Circulation,* 116**,** 1832-44.

TAO, R., COLEMAN, M. C., PENNINGTON, J. D., OZDEN, O., PARK, S. H., JIANG, H., KIM, H. S., FLYNN, C. R., HILL, S., HAYES MCDONALD, W., OLIVIER, A. K., SPITZ, D. R. & GIUS, D. 2010. Sirt3-mediated deacetylation of evolutionarily conserved lysine 122 regulates MnSOD activity in response to stress. *Mol Cell,* 40**,** 893-904.

TAO, Y., YU, S., CHAO, M., WANG, Y., XIONG, J. & LAI, H. 2019. SIRT4 suppresses the PI3K/Akt/NF-κB signaling pathway and attenuates HUVEC injury induced by oxLDL. *Mol Med Rep,* 19**,** 4973-4979.

TARANTINI, S., VALCARCEL-ARES, M. N., TOTH, P., YABLUCHANSKIY, A., TUCSEK, Z., KISS, T., HERTELENDY, P., KINTER, M., BALLABH, P., SÜLE, Z., FARKAS, E., BAUR, J. A., SINCLAIR, D. A., CSISZAR, A. & UNGVARI, Z. 2019. Nicotinamide mononucleotide (NMN) supplementation rescues cerebromicrovascular endothelial function and neurovascular coupling responses and improves cognitive function in aged mice. *Redox Biol,* 24**,** 101192.

TARDIF, J.-C., KOUZ, S., WATERS, D. D., BERTRAND, O. F., DIAZ, R., MAGGIONI, A. P., PINTO, F. J., IBRAHIM, R., GAMRA, H., KIWAN, G. S., BERRY, C., LÓPEZ-SENDÓN, J., OSTADAL, P., KOENIG, W., ANGOULVANT, D., GRÉGOIRE, J. C., LAVOIE, M.-A., DUBÉ, M.-P., RHAINDS, D., PROVENCHER, M., BLONDEAU, L., ORFANOS, A., L'ALLIER, P. L., GUERTIN, M.-C. & ROUBILLE, F. 2019. Efficacy and Safety of Low-Dose Colchicine after Myocardial Infarction. *New England Journal of Medicine,* 381**,** 2497-2505.

TARRAGÓ, M. G., CHINI, C. C. S., KANAMORI, K. S., WARNER, G. M., CARIDE, A., DE OLIVEIRA, G. C., RUD, M., SAMANI, A., HEIN, K. Z., HUANG, R., JURK, D., CHO, D. S., BOSLETT, J. J., MILLER, J. D., ZWEIER, J. L., PASSOS, J. F., DOLES, J. D., BECHERER, D. J. & CHINI, E. N. 2018. A Potent and Specific CD38 Inhibitor Ameliorates Age-Related Metabolic Dysfunction by Reversing Tissue NAD(+) Decline. *Cell Metab,* 27**,** 1081-1095.e10.

TEUPSER, D., PERSKY, A. D. & BRESLOW, J. L. 2003. Induction of Atherosclerosis by Low-Fat, Semisynthetic Diets in LDL Receptor–Deficient C57BL/6J and FVB/NJ Mice. *Arteriosclerosis, Thrombosis, and Vascular Biology,* 23**,** 1907-1913.

TORRES-CASTRO, I., ARROYO-CAMARENA, Ú. D., MARTÍNEZ-REYES, C. P., GÓMEZ-ARAUZ, A. Y., DUEÑAS-ANDRADE, Y., HERNÁNDEZ-RUIZ, J., BÉJAR, Y. L., ZAGA-CLAVELLINA, V., MORALES-MONTOR, J.,

TERRAZAS, L. I., KZHYSHKOWSKA, J. & ESCOBEDO, G. 2016. Human monocytes and macrophages undergo M1-type inflammatory polarization in response to high levels of glucose. *Immunology Letters,* 176**,** 81-89.

TSENG, A. H., SHIEH, S. S. & WANG, D. L. 2013. SIRT3 deacetylates FOXO3 to protect mitochondria against oxidative damage. *Free Radic Biol Med,* 63**,** 222-34.

USUI, F., SHIRASUNA, K., KIMURA, H., TATSUMI, K., KAWASHIMA, A., KARASAWA, T., HIDA, S., SAGARA, J., TANIGUCHI, S. I. & TAKAHASHI, M. 2012. Critical role of caspase-1 in vascular inflammation and development of atherosclerosis in Western diet-fed apolipoprotein E-deficient mice. *Biochemical and Biophysical Research Communications,* 425**,** 162-168.

VAN DIJK, R. A., KLEEMANN, R., SCHAAPHERDER, A. F., VAN DEN BOGAERDT, A., HEDIN, U., MATIC, L. & LINDEMAN, J. H. N. 2023. Validating human and mouse tissues commonly used in atherosclerosis research with coronary and aortic reference tissue: similarities but profound differences in disease initiation and plaque stability. *JVS Vasc Sci,* 4**,** 100118.

VAN GOOL, F., GALLI, M., GUEYDAN, C., KRUYS, V., PREVOT, P. P., BEDALOV, A., MOSTOSLAVSKY, R., ALT, F. W., DE SMEDT, T. & LEO, O. 2009. Intracellular NAD levels regulate tumor necrosis factor protein synthesis in a sirtuin-dependent manner. *Nat Med,* 15**,** 206-10.

VARGHESE, G. P., FOLKERSEN, L., STRAWBRIDGE, R. J., HALVORSEN, B., YNDESTAD, A., RANHEIM, T., KROHG‐SØRENSEN, K., SKJELLAND, M., ESPEVIK, T., AUKRUST, P., LENGQUIST, M., HEDIN, U., JANSSON, J. H., FRANSÉN, K., HANSSON, G. K., ERIKSSON, P. & SIRSJÖ, A. 2016. NLRP3 Inflammasome Expression and Activation in Human Atherosclerosis. *Journal of the American Heart Association,* 5**,** e003031.

VENTER, G., OERLEMANS, F. T., WILLEMSE, M., WIJERS, M., FRANSEN, J. A. & WIERINGA, B. 2014. NAMPT-mediated salvage synthesis of NAD+ controls morphofunctional changes of macrophages. *PLoS One,* 9**,** e97378.

VIRMANI, R., KOLODGIE, F. D., BURKE, A. P., FINN, A. V., GOLD, H. K., TULENKO, T. N., WRENN, S. P. & NARULA, J. 2005. Atherosclerotic Plaque Progression and Vulnerability to Rupture. *Arteriosclerosis, Thrombosis, and Vascular Biology,* 25**,** 2054-2061.

WANG, Y., DUBLAND, J. A., ALLAHVERDIAN, S., ASONYE, E., SAHIN, B., JAW, J. E., SIN, D. D., SEIDMAN, M. A., LEEPER, N. J. & FRANCIS, G. A. 2019. Smooth Muscle Cells Contribute the Majority of Foam Cells in ApoE (Apolipoprotein E)-Deficient Mouse Atherosclerosis. *Arteriosclerosis, Thrombosis, and Vascular Biology,* 39**,** 876-887.

WARBURG, O. & CHRISTIAN, W. 1936. Pyridin, der wasserstoffübertragende Bestandteil von Gärungsfermenten. *Helvetica Chimica Acta,* 19**,** E79-E88.

WEI, T., GAO, J., HUANG, C., SONG, B., SUN, M. & SHEN, W. 2021. SIRT3 (Sirtuin-3) Prevents Ang II (Angiotensin II)–Induced Macrophage Metabolic Switch Improving Perivascular Adipose Tissue Function. *Arteriosclerosis, Thrombosis, and Vascular Biology,* 41**,** 714-730.

WHITSON, J. A., BITTO, A., ZHANG, H., SWEETWYNE, M. T., COIG, R., BHAYANA, S., SHANKLAND, E. G., WANG, L., BAMMLER, T. K., MILLS, K. F., IMAI, S.-I., CONLEY, K. E., MARCINEK, D. J. & RABINOVITCH, P. S. 2020. SS-31 and NMN: Two paths to improve metabolism and function in aged hearts. *Aging Cell,* 19**,** e13213.

WINZELL, M. S. R. & AHRÉN, B. 2004. The High-Fat Diet–Fed Mouse: A Model for Studying Mechanisms and Treatment of Impaired Glucose Tolerance and Type 2 Diabetes. *Diabetes,* 53**,** S215-S219.

WU, L., VIKRAMADITHYAN, R., YU, S., PAU, C., HU, Y., GOLDBERG, I. J. & DANSKY, H. M. 2006. Addition of dietary fat to cholesterol in the diets of LDL receptor knockout mice: effects on plasma insulin, lipoproteins, and atherosclerosis. *J Lipid Res,* 47**,** 2215-22.

YAMANE, T., IMAI, M., BAMBA, T. & UCHIYAMA, S. 2023. Nicotinamide mononucleotide (NMN) intake increases plasma NMN and insulin levels in healthy subjects. *Clinical Nutrition ESPEN,* 56**,** 83-86.

YI, L., MAIER, A. B., TAO, R., LIN, Z., VAIDYA, A., PENDSE, S., THASMA, S., ANDHALKAR, N., AVHAD, G. & KUMBHAR, V. 2023. The efficacy and safety of β-nicotinamide mononucleotide (NMN) supplementation in healthy middle-aged adults: a randomized, multicenter, double-blind, placebo-controlled, parallel-group, dose-dependent clinical trial. *GeroScience,* 45**,** 29-43.

YOSHINO, J., BAUR, J. A. & IMAI, S. I. 2018. NAD(+) Intermediates: The Biology and Therapeutic Potential of NMN and NR. *Cell Metab,* 27**,** 513-528.

YOSHINO, J., MILLS, K. F., YOON, M. J. & IMAI, S. 2011. Nicotinamide mononucleotide, a key NAD(+) intermediate, treats the pathophysiology of diet- and age-induced diabetes in mice. *Cell Metab,* 14**,** 528-36.

YOSHINO, M., YOSHINO, J., KAYSER, B. D., PATTI, G. J., FRANCZYK, M. P., MILLS, K. F., SINDELAR, M., PIETKA, T., PATTERSON, B. W., IMAI, S. I. & KLEIN, S. 2021. Nicotinamide mononucleotide increases muscle insulin sensitivity in prediabetic women. *Science,* 372**,** 1224-1229.

YU, W., DITTENHAFER-REED, K. E. & DENU, J. M. 2012. SIRT3 protein deacetylates isocitrate dehydrogenase 2 (IDH2) and regulates mitochondrial redox status. *J Biol Chem,* 287**,** 14078-86.

ZHAI, X., HAN, W., WANG, M., GUAN, S. & QU, X. 2019. Exogenous supplemental NAD+ protect myocardium against myocardial ischemic/reperfusion injury in swine model. *Am J Transl Res,* 11**,** 6066-6074.

ZHANG, B., MA, Y. & XIANG, C. 2018a. SIRT2 decreases atherosclerotic plaque formation in low-density lipoprotein receptor-deficient mice by modulating macrophage polarization. *Biomedicine & Pharmacotherapy,* 97**,** 1238-1242.

ZHANG, H., HEAD, P. E. & YU, D. S. 2016. SIRT2 orchestrates the DNA damage response. *Cell Cycle,* 15**,** 2089-2090.

ZHANG, J., XIANG, H., LIU, J., CHEN, Y., HE, R. R. & LIU, B. 2020. Mitochondrial Sirtuin 3: New emerging biological function and therapeutic target. *Theranostics,* 10**,** 8315-8342.

ZHANG, Q. J., WANG, Z., CHEN, H. Z., ZHOU, S., ZHENG, W., LIU, G., WEI, Y. S., CAI, H., LIU, D. P. & LIANG, C. C. 2008. Endothelium-specific overexpression of class III deacetylase SIRT1 decreases atherosclerosis in apolipoprotein E-deficient mice. *Cardiovasc Res,* 80**,** 191-9.

ZHANG, R., CHEN, S., WANG, Z., YE, L., JIANG, Y., LI, M., JIANG, X., PENG, H., GUO, Z., CHEN, L., ZHANG, R., NIU, Y., ASCHNER, M., LI, D. & CHEN, W. 2023. Assessing the Effects of Nicotinamide Mononucleotide Supplementation on Pulmonary Inflammation in Male Mice Subchronically Exposed to Ambient Particulate Matter. *Environ Health Perspect,* 131**,** 77006.

ZHANG, S., WEINBERG, S., DEBERGE, M., GAINULLINA, A., SCHIPMA, M., KINCHEN, J. M., BEN-SAHRA, I., GIUS, D. R., YVAN-CHARVET, L.,

CHANDEL, N. S., SCHUMACKER, P. T. & THORP, E. B. 2019. Efferocytosis Fuels Requirements of Fatty Acid Oxidation and the Electron Transport Chain to Polarize Macrophages for Tissue Repair. *Cell Metab,* 29**,** 443-456.e5.

ZHANG, X., SESSA, W. C. & FERNÁNDEZ-HERNANDO, C. 2018b. Endothelial Transcytosis of Lipoproteins in Atherosclerosis. *Front Cardiovasc Med,* 5**,** 130.

ZHENG, F., XING, S., GONG, Z., MU, W. & XING, Q. 2014. Silence of NLRP3 suppresses atherosclerosis and stabilizes plaques in apolipoprotein E-deficient mice. *Mediators Inflamm,* 2014**,** 507208.

ZHENG, F., XING, S., GONG, Z. & XING, Q. 2013. NLRP3 inflammasomes show high expression in aorta of patients with atherosclerosis. *Heart Lung Circ,* 22**,** 746-50.

ZHENG, J., CHEN, K., WANG, H., CHEN, Z., XI, Y., YIN, H., LAI, K. & LIU, Y. 2018. SIRT7 Regulates the Vascular Smooth Muscle Cells Proliferation and Migration via Wnt/β-Catenin Signaling Pathway. *Biomed Res Int,* 2018**,** 4769596.

ZHOU, B., WANG, D. D., QIU, Y., AIRHART, S., LIU, Y., STEMPIEN-OTERO, A., O'BRIEN, K. D. & TIAN, R. 2020. Boosting NAD level suppresses inflammatory activation of PBMCs in heart failure. *J Clin Invest,* 130**,** 6054-6063.

ZHOU, L., WANG, F., SUN, R., CHEN, X., ZHANG, M., XU, Q., WANG, Y., WANG, S., XIONG, Y., GUAN, K. L., YANG, P., YU, H. & YE, D. 2016. SIRT5 promotes IDH2 desuccinylation and G6PD deglutarylation to enhance cellular antioxidant defense. *EMBO Rep,* 17**,** 811-22.

Eurostat 2023: Causes of death - deaths by country of residence and occurrence. Available from https://ec.europa.eu/eurostat/databrowser/view/hlth_cd_aro/default/table?lang=en[01.11.23]

12 Supplemental data

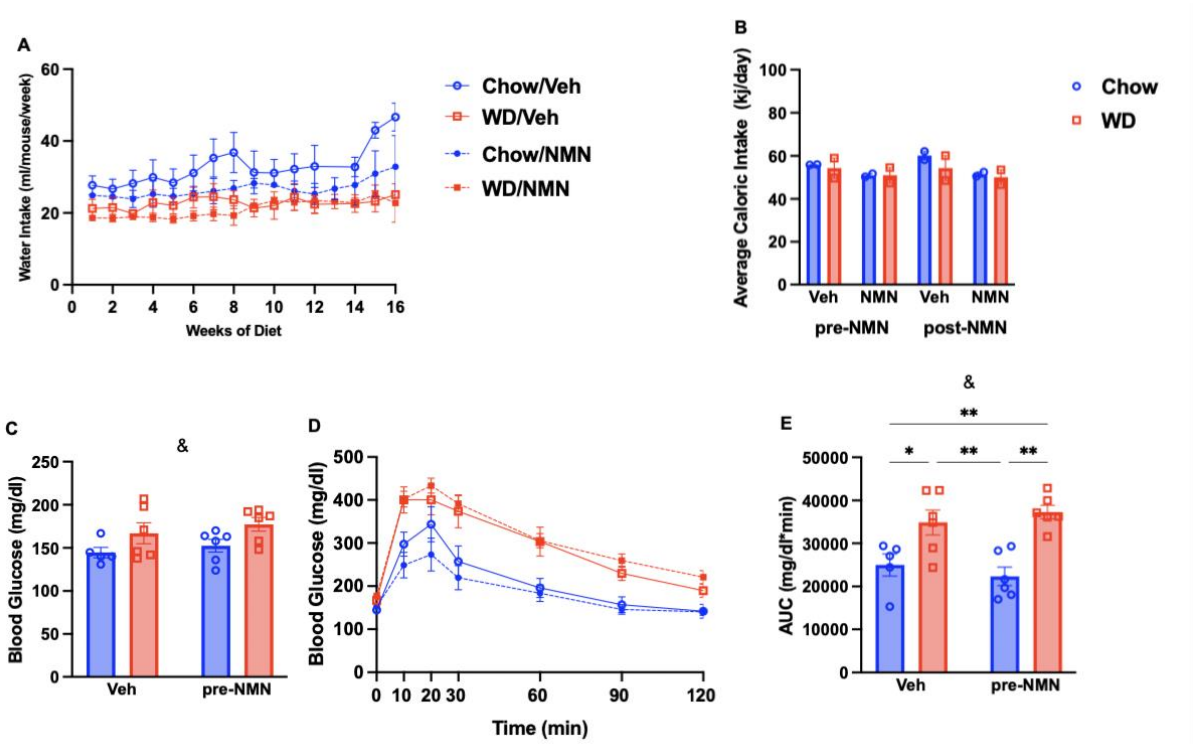

Supplemental figure 1: NMN-treatment did not affect water or caloric intake. A) daily water intake per mouse per day, B) average caloric intake per mouse per day (n=2), C) fasting blood glucose levels after 8 weeks of diet, D) iGTT after 8 weeks of diet, E) AUC of iGTT in Chow- and WD-fed Ldlr$^{-/-}$ mice treated with Veh or NMN (n=5-6). 2 way-ANOVA: &=effect of diet; ∗ p<0.05, ∗∗ p<0.01 using post-hoc tests. AUC, area under the curve; iGTT, intraperitoneal glucose tolerance test; Ldlr$^{-/-}$, low-density lipoprotein receptor knockout; NMN, nicotinamide mononucleotide; Veh, vehicle. WD, western diet.

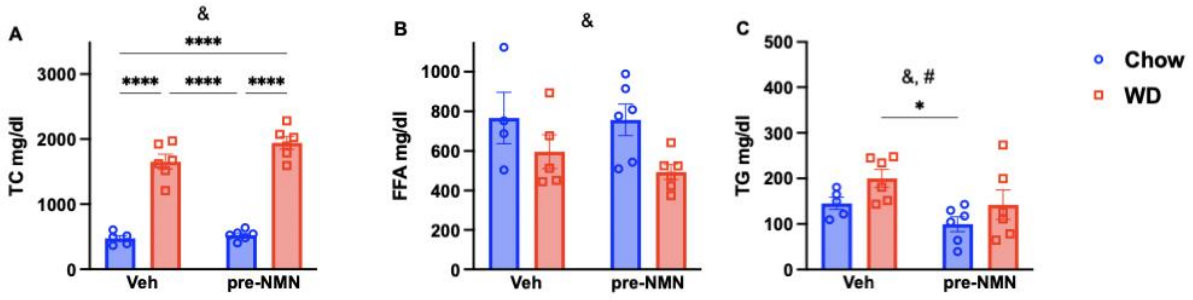

Supplemental figure 2: WD-diet increased TC and TG levels, but reduced FFA levels, after 8 weeks of feeding. The TG-levels of the groups which were started on NMN were slightly reduced compared to their counterparts. A) TC, B) and C) TG concentrations in plasma after 8 weeks of diet in Chow- and WD-fed Ldlr$^{-/-}$ mice treated with Veh or NMN (n=5-6). 2 way-ANOVA: &=effect of diet, #=effect of treatment; ∗ p<0.05, ∗∗∗∗ p<0.0001 using post-hoc tests. FFA, free fatty acids; Ldlr$^{-/-}$, low-density lipoprotein receptor knockout**;** NMN, nicotinamide mononucleotide; TC, total cholesterol; TG, triglycerides; Veh, vehicle; WD, western diet.